Energy Bands for $KNiF_3$, $SrTiO_3$, $KMoO_3$, and $KTaO_3$

L. F. Mattheiss
Bell Laboratories, Murray Hill, New Jersey 07974
(Received 26 May 1972)

The nonrelativistic augmented-plane-wave (APW) method has been applied to calculate the electronic band structures for several cubic perovskite-type compounds, including $KNiF_3$, $SrTiO_3$, $KMoO_3$, and $KTaO_3$. These calculations involve *ad hoc* crystal potentials that are derived from neutral-atom charge densities. The energy-band results for the $2p$ valence bands and the t_{2g}-e_g conduction bands in these ternary compounds are similar to the tight-binding results of Kahn and Leyendecker for $SrTiO_3$ and the previous APW results for ReO_3. It is found that the additional conduction bands associated with the metal s-p and the potassium or strontium d orbitals lie several electron volts above the Fermi level for each compound. The APW results for the $2s$-$2p$ valence bands and the lowest t_{2g}-e_g conduction bands have been fitted with the Slater and Koster linear-combination-of-atomic-orbitals (LCAO) interpolation scheme, including orbital-overlap effects. The LCAO parameters which determine the p-d band gaps in the oxides have been adjusted in accordance with optical and cyclotron-mass data. Assuming a rigid-band model and including spin-orbit effects, this adjusted LCAO model is applied to calculate constant-energy surfaces, cyclotron masses, and density-of-states curves for the n-type semiconductors $SrTiO_3$ and $KTaO_3$ as well as the nonstoichiometric metallic bronze $K_{0.92}MoO_3$. It is found that (a) the conduction bands in n-type $SrTiO_3$ and $KTaO_3$ consist of warped bands at the zone center rather than many valleys at X, as Kahn and Leyendecker have proposed; (b) the fundamental p-d band gaps in both $SrTiO_3$ and $KTaO_3$ are direct; (c) the LCAO joint-density-of-states results for $SrTiO_3$ and $KTaO_3$ provide a qualitative interpretation of the optical data; (d) the calculated extremal areas for orbits on the $K_{0.92}MoO_3$ Fermi surface agree to within 10% with recent de Haas–van Alphen data.

I. INTRODUCTION

There has been a long-term interest in the perovskite-type compounds with chemical formula ABC_3 because of their unusual magnetic[1] and dielectric[2] properties. Although there are more than a hundred compounds with this structure, the recent interest has been focussed primarily on $SrTiO_3$ and other closely related oxides. To a large extent, this interest has been stimulated by the results of a band-structure calculation by Kahn and Leyendecker[3] (KL) and the observation of superconductivity in semiconducting samples of $SrTiO_3$ by Schooley *et al.*[4]

The KL band-structure calculation for $SrTiO_3$ was semiempirical in nature and involved the tight-binding or linear-combination-of-atomic-orbitals (LCAO) method of Slater and Koster.[5] It predicts that the lowest conduction bands in $SrTiO_3$ involve the titanium t_{2g} orbitals and that the energy minima are located at or near the Brillouin-zone boundaries along the ⟨100⟩ directions. Cohen[6] had previously predicted that such a many-valley model was favorable for the occurrence of superconductivity in semiconductors and semimetals.

The purpose of the present investigation is to provide a detailed theoretical model for the band structures of several cubic perovskite-type compounds and to compare these energy-band results with the existing experimental data. These calculations have been carried out on four compounds, $KNiF_3$, $SrTiO_3$, $KMoO_3$, and $KTaO_3$. The first compound, $KNiF_3$, is an antiferromagnetic insulator with a Néel temperature of 275 °K. Optical-absorption studies suggest that it is more appropriate to treat the nickel $3d$ electrons in $KNiF_3$ in terms of ligand-field theory rather than one-electron band theory. There have been numerous applications of the molecular-orbital (MO) method to calculate the electronic structure of a single $(NiF_6)^{4-}$ octahedral complex,[7] but there have been no previous band-structure calculations for this compound.

Among the oxide compounds, both $SrTiO_3$ and $KTaO_3$ are insulators with band gaps of about 3.5 eV separating the filled oxygen $2p$ bands from the empty titanium or tantalum t_{2g} bands. Both compounds can be made into n-type semiconductors by doping or reduction. Strontium titanate undergoes a cubic-to-tetragonal structural transformation near 110 °K, and there is some evidence for the occurrence of additional phase transitions at lower temperatures.[8] It is believed that $KTaO_3$ remains cubic down to 1 °K. In addition to the KL calculation, Soules *et al.*[9] have recently carried out a self-consistent MO-type calculation for $SrTiO_3$ using the Hartree–Fock–Roothaan procedure.

Finally, $K_{0.92}MoO_3$ is a nonstoichiometric metallic bronze that is nearly isoelectronic with ReO_3, containing 0.92 rather than one electron in the t_{2g} conduction bands. It appears to remain cubic down to 4.2 °K, though there are some indications that

a similar compound, $Na_{0.93}MoO_3$, may undergo a noncubic distortion at low temperatures.[10] Marcus and Bither[10] have observed the de Haas–van Alphen effect in both these bronzes and find that these data exhibit many similarities with the earlier ReO_3 results.[11,12]

The general methods that are utilized in the present investigation have been applied previously in similar band-structure calculations for ReO_3[13,14] and the $3d$ transition-metal monoxides.[15,16] The calculations are carried out in three stages. In the first stage, the augmented-plane-wave (APW) method is applied to calculate the energy-band results at symmetry points in the Brillouin zone. These APW results are then used to determine various parameters in the Slater–Koster LCAO interpolation scheme which is applied to fit the valence- and lowest-conduction-band states. Finally, the LCAO parameters which determine the p-d band gaps in these compounds are adjusted in accordance with optical and cyclotron-mass data.

The various details that are involved in these APW and LCAO calculations are described in Sec. II. The results of the combined APW-LCAO calculations are presented in Sec. III, which includes energy-band and density-of-states curves, Fermi-surface cross sections, cyclotron-mass results, and LCAO parameters for $KNiF_3$, $SrTiO_3$, $KMoO_3$, and $KTaO_3$. These theoretical results are compared with experiment in Sec. IV. However, a detailed discussion of some of the low-temperature data for $SrTiO_3$ is postponed to the following paper,[17] where the present LCAO model for cubic $SrTiO_3$ is generalized and applied to predict the effect of the cubic-to-tetragonal structural transition on the $SrTiO_3$ conduction bands. The final section includes a general discussion of the present results and a detailed comparison with other band models that have been proposed for these perovskite-type compounds.

II. DETAILS OF CALCULATION

A. Perovskite Structure

The primitive cell for the ideal perovskite structure ABC_3 is illustrated in Fig. 1(a). It contains a B atom at the origin, C atoms at each of the face centers, and A atoms at the corners of the simple cubic unit cell. Each cell contains a single ABC_3 complex. The space group is O_h^1 and the Bravais lattice is simple cubic. The corresponding Brillouin zone is shown to the right in Fig. 1(b), where the standard notation is used to label symmetry points and lines. Both the A and B atoms are situated at sites with full cubic (O_h) point symmetry, while the C-atom sites have tetragonal (D_{4h}) symmetry. If the A atoms are removed from the perovskite structure, the remaining array of

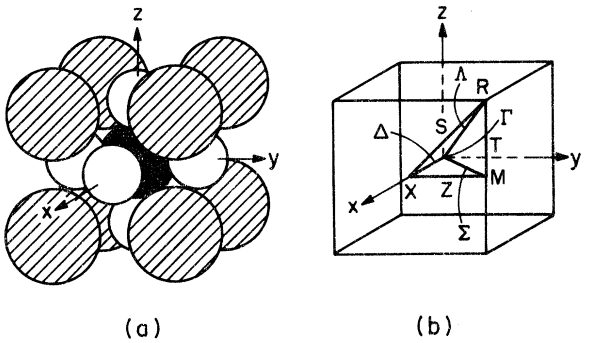

FIG. 1. (a) Unit cell for the perovskite-type ABC_3 compounds, where the A atoms are shaded, the B atom is filled, and the C atoms are unshaded. (b) Brillouin zone for the simple cubic Bravais lattice.

BC_3 atoms form the ReO_3 structure.

To aid in identifying the atomic origin of various groups of energy-band states, it is useful to determine the symmetry properties of Bloch sums formed from s, p, and d orbitals that are localized at the A, B, and C sites, respectively. These results are already available for orbitals at both the B and C sites.[3,13] The corresponding results for orbitals at the A site are compared with those for the B site in Table I. It is noted that although the symmetries of the A- and B-atom s, p, and d states are identical at Γ, they do differ at other symmetry points in the Brillouin zone. These differences often allow one to determine the atomic origin of a given energy-band state without a detailed examination of the APW wave function.

B. APW Calculations

The present APW results are based on *ad hoc* crystal potentials that are derived from the Hartree–Fock–Slater atomic charge densities of Herman and Skillman.[18] As in previous calculations,[13,15] the approximate crystal potential $V(\vec{r})$ is separated into a muffin-tin part $V_m(\vec{r})$ plus corrections $V_\Delta(\vec{r})$. These corrections $V_\Delta(\vec{r})$ take into account exactly the variations in $V(\vec{r})$ outside the various APW spheres, but they neglect the nonspherical corrections to $V_m(\vec{r})$ within the individual APW spheres. Exchange effects are introduced using Slater's original free-electron exchange approximation.[19] The detailed numerical methods that are used to calculate $V_m(\vec{r})$ and the Fourier coefficients of the corrections $V_\Delta(\vec{K}_j)$ are identical with those involved in the previous ReO_3 calculation.[13]

The values for the lattice parameters and the various APW sphere radii that are involved in the present calculations are listed in Table II. The radii of the B- and C-atom spheres were chosen so they touched along the ⟨100⟩ directions. In addition, the ratio of these radii, R_B/R_C, has been

TABLE I. Symmetry properties of Bloch sums formed from s, p, and d orbitals centered at the A and B sites of the perovskite-type ABC_3 compounds with the origin at a B site.

Orbital	Γ	X	M	R
A-atom s	Γ_1	X_4'	M_3	R_2'
A-atom p	Γ_{15}	X_1+X_5	$M_2'+M_5'$	R_{25}'
A-atom d	$\Gamma_{12}+\Gamma_{25}'$	$X_2'+X_3'+X_4'+X_5'$	$M_1+M_3+M_4+M_5$	$R_{12}'+R_{15}$
B-atom s	Γ_1	X_1	M_1	R_1
B-atom p	Γ_{15}	$X_4'+X_5'$	$M_4'+M_5'$	R_{15}
B-atom d	$\Gamma_{12}+\Gamma_{25}'$	$X_1+X_2+X_3+X_5$	$M_1+M_2+M_3+M_5$	$R_{12}+R_{25}'$

arbitrarily set equal to $\frac{7}{6}$ in order to equalize the relative convergence of the APW eigenvalues for states associated with the B-atom d bands and the C-atom p bands.[20] With this choice for R_B and R_C, the A-atom sphere radii, R_A, can be made quite large. In fact, to obtain touching A- and C-atom spheres along $\langle 110\rangle$, one must set $R_A = 0.476a$, which is quite close to the value ($R_A = \frac{1}{2}a$) for a simple cubic lattice of touching A-atom spheres.

In the actual APW calculations, a reduced value for $R_A \approx 0.4a = 2.95$ a.u. has been used for each compound. With this reduced value for R_A, approximately 50% of the unit-cell volume is contained within the five APW spheres. This is to be compared with the maximum value of 69% for touching spheres and a value of 24% for the ReO_3 structure. The use of a reduced value for R_A minimizes the nonspherical corrections to the potential within the A-atom spheres without adversely affecting the relative convergence of these states. In each compound, this radius falls quite near the maximum in the potential $V(\vec{r})$ that occurs along the line joining the nearest-neighbor A- and C-atom sites.

The corrections to the muffin-tin potential $V_\Delta(\vec{r})$ are somewhat smaller in these perovskite-type compounds than they were in the case of ReO_3.[13] Relative to the muffin-tin constant, these corrections range from about -0.8 to $+0.3$ Ry in $KNiF_3$, from -1.1 to $+0.3$ Ry in $SrTiO_3$, and from -1.5 to $+0.5$ Ry in both $KMoO_3$ and $KTaO_3$. The corresponding range for $V_\Delta(\vec{r})$ in ReO_3 was from -2.1 to $+0.7$ Ry. This reduction in $V_\Delta(\vec{r})$ is reflected in the relative magnitudes of the Fourier coefficients $V_\Delta(\vec{K}_j)$. This is shown in Table III, where the first few Fourier coefficients $V_\Delta(\vec{K}_j)$ for the perovskites and ReO_3 are compared. In general, the values of $V_\Delta(\vec{K}_j)$ for the perovskites are reduced by factors of 2–6 when compared with those for ReO_3.

It is particularly important to include these corrections $V_\Delta(\vec{r})$ in the APW calculations for $SrTiO_3$ and $KTaO_3$. According to the KL model and the results of Sec. III, the Fermi level in n-type $SrTiO_3$ and $KTaO_3$ occurs within a band whose width along the Δ direction is about 0.01 Ry. Thus, in order to make a meaningful prediction as to whether the conduction-band minimum occurs at Γ or X, one requires a relative accuracy at both points which is better than 0.01 Ry. This type of accuracy would be difficult to justify in the muffin-tin approximation when deviations from the constant part of the potential are of the order of 1 Ry.

C. LCAO Model

The Slater and Koster[5] LCAO method involving nonorthogonal orbitals is applied to fit the APW results at Γ, X, M, and R for the valence- and lowest-conduction-band states. This simplified LCAO model involves the B-atom d orbitals and the C-atom $2s$ and $2p$ orbitals. It neglects the B-atom s-p orbitals as well as all orbitals associated with the A atom.

The nonzero elements of the energy and overlap matrices involving these orbitals are contained in Table III of Ref. 13 and Table I of Ref. 14, respectively. Some modifications and simplifications of this LCAO model have been made in the present

TABLE II. Lattice parameters and APW sphere radii for ABC_3 compounds with the perovskite structure.

ABC_3	a(Å)	a(a.u.)	R_A(a.u.)	R_B(a.u.)	R_C(a.u.)
$KNiF_3$	4.014[a]	7.585	2.9500	2.0422	1.7505
$SrTiO_3$	3.9051[b]	7.3797	2.9500	1.9868	1.7030
$K_{0.92}MoO_3$	3.919[c]	7.406	2.9500	1.9939	1.7091
$KTaO_3$	3.9884[b]	7.5371	2.9500	2.0292	1.7393
ReO_3	3.7415[d]	7.0705	···	1.9035	1.6317

[a]A. Okazaki and Y. Suemune, J. Phys. Soc. Japan 16, 671 (1961).

[b]R. W. G. Wyckoff, *Crystal Structures* II (Interscience, New York, 1964).

[c]Reference 10.

[d]W. B. Pearson, in *A Handbook of Lattice Spacings and Structures of Metals and Alloys* (Pergamon, New York, 1958).

TABLE III. Comparison between the low-order Fourier coefficients $V_\Delta(\vec{K}_j)$ for several perovskite-type compounds and ReO_3.

	$V_\Delta(\vec{K}_j)$ (Ry)				
$\vec{K}_j(2\pi/a)$	$KNiF_3$	$SrTiO_3$	$KMoO_3$	$KTaO_3$	ReO_3
(1,0,0)	−0.020	−0.026	−0.041	−0.044	−0.128
(1,1,0)	−0.009	−0.014	−0.022	−0.024	0.013
(1,1,1)	0.016	0.020	0.027	0.029	0.017
(2,0,0)	0.005	0.009	0.018	0.018	0.048
(2,1,0)	0.001	0.002	0.007	0.008	0.028
(2,1,1)	0.004	0.008	0.013	0.013	0.002
(2,2,0)	0.014	0.015	0.020	0.020	0.023
(3,0,0)	0.011	0.014	0.018	0.017	0.021

TABLE IV. Comparison between tight-binding integrals and LCAO parameters involved in the present LCAO model for perovskite-type compounds and two earlier models for ReO_3.

Integral		Two-center approx.	ReO_3 LCOAO	ReO_3 LCAO	Perovskite LCAO
$E_{s1,s1}$	(0, 0, 0)	E_s	···	E_s	E_s
$E_{s1,s2}$	$(\frac{1}{2},\frac{1}{2},0)$	$(ss\sigma)$	···	···	$(ss\sigma)$
$E_{x1,x1}$	(0, 0, 0)	E_{pa}	A_1	A_1	E_{pa}
$E_{x1,x1}$	(1, 0, 0)	$(pp\sigma)_2$	A_2	A_2	$(pp\sigma)_2$
$E_{x1,x1}$	(0, 1, 0)	$(pp\pi)_2$	A_3	A_3	$(pp\pi)_2$
$E_{y1,y1}$	(0, 0, 0)	$E_{p\pi}$	B_1	B_1	$E_{p\pi}$
$E_{y1,y1}$	(1, 0, 0)	$(pp\pi)_2$	B_2	B_2	$(pp\pi)_2$
$E_{y1,y1}$	(0, 1, 0)	$(pp\sigma)_2$	B_3	B_3	$(pp\sigma)_2$
$E_{y1,y1}$	(0, 0, 1)	$(pp\pi)_2$	B_4	B_4	$(pp\pi)_2$
$E_{x1,x2}$	$(\frac{1}{2},\frac{1}{2},0)$	$\frac{1}{2}[(pp\sigma)_1+(pp\pi)_1]$	C_1	C_1	C_1
$E_{x1,y2}$	$(\frac{1}{2},\frac{1}{2},0)$	$\frac{1}{2}[(pp\sigma)_1-(pp\pi)_1]$	C_2	C_2	C_2
$E_{y1,x2}$	$(\frac{1}{2},\frac{1}{2},0)$	$\frac{1}{2}[(pp\sigma)_1-(pp\pi)_1]$	C_3	C_3	C_3
$E_{z1,z2}$	$(\frac{1}{2},\frac{1}{2},0)$	$(pp\pi)_1$	C_4	C_4	C_4
$E_{xy,xy}$	(0, 0, 0)	$E_{d\pi}$	D_1	D_1	E_d
$E_{xy,xy}$	(1, 0, 0)	$(dd\pi)$	···	···	···
$E_{xy,xy}$	(0, 0, 1)	$(dd\delta)$	D_3	D_3	D_3
$E_{3z^2-r^2,3z^2-r^2}$	(0, 0, 0)	$E_{d\sigma}$	D_4	D_4	E_d
$E_{3z^2-r^2,3z^2-r^2}$	(0, 0, 1)	$(dd\sigma)$	D_5	D_5	···
$E_{x^2-y^2,x^2-y^2}$	(0, 0, 1)	$(dd\delta)$	D_6	D_6	D_6
$S_{s3,3z^2-r^2}$	$(0,0,\frac{1}{2})$	S_s	···	S_s	S_s
$E_{s3,3z^2-r^2}$	$(0,0,\frac{1}{2})$	$(sd\sigma)$	···	$(sd\sigma)$	$(sd\sigma)$
$S_{z3,3z^2-r^2}$	$(0,0,\frac{1}{2})$	S_σ	···	S_σ	S_σ
$E_{z3,3z^2-r^2}$	$(0,0,\frac{1}{2})$	$(pd\sigma)$	P_2	$(pd\sigma)$	$(pd\sigma)$
$S_{x2,xy}$	$(0,\frac{1}{2},0)$	S_π	···	···	S_π
$E_{x2,xy}$	$(0,\frac{1}{2},0)$	$(pd\pi)$	P_1	$(pd\pi)$	$(pd\pi)$
Total no. of parameters			18	21	19

application to the perovskite-type compounds. These are summarized in Table IV, where we distinguish between the LCAO[14] and linear-combination-of-"orthogonalized"-atomic-orbitals[13] (LCOAO) methods. In the present LCAO model, we have added a two-center energy parameter $(ss\sigma)$ involving nearest-neighbor C-atom $2s$ interactions to improve the LCAO fit to the $2s$ bands. In addition, the second-neighbor $2p$-$2p$ interactions A_2, A_3, B_2-B_4 have been reduced to the two-center approximation so that $A_2 = B_3 = (pp\sigma)_2$ and $A_3 = B_2 = B_4 = (pp\pi)_2$.

A nonlinear least-squares fitting procedure has been applied to determine the LCAO parameters from the APW eigenvalues at symmetry points in the Brillouin zone.[15] This technique is superior to the two-step process that was applied originally to determine the LCOAO parameters for ReO_3[13] since the fitting procedure treats all 40 APW energy levels for the C-atom $2s$-$2p$ and the B-atom d bands in an equivalent manner.

In applying this nonlinear least-squares method, it was found that the LCAO parameters A_2, A_3, and B_2-B_4 could not be determined uniquely from the APW results at Γ, X, M, R. However, it was found that these parameters could be determined if they were reduced to the two-center approximation. Similar difficulties were experienced in determining the d-orbital energies $E_{d\sigma}$ and $E_{d\pi}$ as well as the nearest-neighbor d-d interaction parameters $D_2((dd\pi))$ and $D_5((dd\sigma))$. These problems are due to the difficulty in separating the direct and indirect contributions to the effective d-d LCAO interaction parameters (see Table V of Ref. 15). To resolve this ambiguity in the simplest possible manner, we have arbitrarily set $E_{d\sigma} = E_{d\pi} = E_d$ and neglected both $(dd\sigma)$ and $(dd\pi)$ in the present LCAO model.

III. RESULTS

The APW results along the Δ direction of the Brillouin zone for $KNiF_3$, $SrTiO_3$, $KMoO_3$, $KTaO_3$, and ReO_3 are compared in Fig. 2. Since the APW calculations have been carried out only at the end points, the solid lines represent only estimates to the actual band profiles. The zero of energy for each compound has been adjusted so it coincides with the upper Γ_{15} state in the C-atom $2p$ bands. Situated below this group of nine $2p$ bands are the narrow potassium (strontium) $3p$ ($4p$) core states, which are absent in ReO_3. The lowest group of three bands originate from the C-atom $2s$ orbitals.

A similar identification of the various groups of bands at positive energies is possible. The lowest five bands correspond to the antibonding (with respect to the C-atom s and p orbitals) B-atom t_{2g} (xy, yz, zx) and $e_g(3z^2-r^2, x^2-y^2)$ orbitals which evolve from $\Gamma_{25'}$ and Γ_{12}, respectively. Just above the e_g bands, we find the bottom of the antibonding s-p conduction bands (Γ_1) as well as the A-atom d bands (Γ_{12} and $\Gamma_{25'}$). Again, the latter are absent in ReO_3.

The results of the APW calculations at Γ, X, M, and R for $KNiF_3$, $SrTiO_3$, $KMoO_3$, $KTaO_3$, and ReO_3 are listed in Table V. The 40 APW eigenvalues for the C-atom $2s$-$2p$ bands and the B-atom d bands have been used to determine 19 LCAO parameters, as described in Sec. IIIC. The values for these LCAO parameters are listed in Table VI. The rms and maximum errors in the LCAO fit to the APW results are listed below each set of parameters.

The over-all accuracy of this LCAO fit to the APW results is shown in Figs. 3–6, where we plot the LCAO bands as solid lines and represent the APW energy eigenvalues as open circles for $KNiF_3$ (Fig. 3), $SrTiO_3$ (Fig. 4), $KMoO_3$ (Fig. 5), and $KTaO_3$ (Fig. 6). In these figures, the dashed lines represent additional bands that are not included in this simplified LCAO model. The A-atom $3p$-$4p$ core states of Fig. 2 and Table V are omitted from these figures.

The density-of-states curves shown to the right in Figs. 3–6 are obtained by sampling the LCAO bands at 32 768 uniformly distributed points in the Brillouin zone. The Fermi level in nonmagnetic $KNiF_3$ would occur at $E = 0.635$ Ry, in the middle of the nickel e_g bands. The corresponding Fermi levels for $SrTiO_3$ and $KTaO_3$ occur in the p-d band

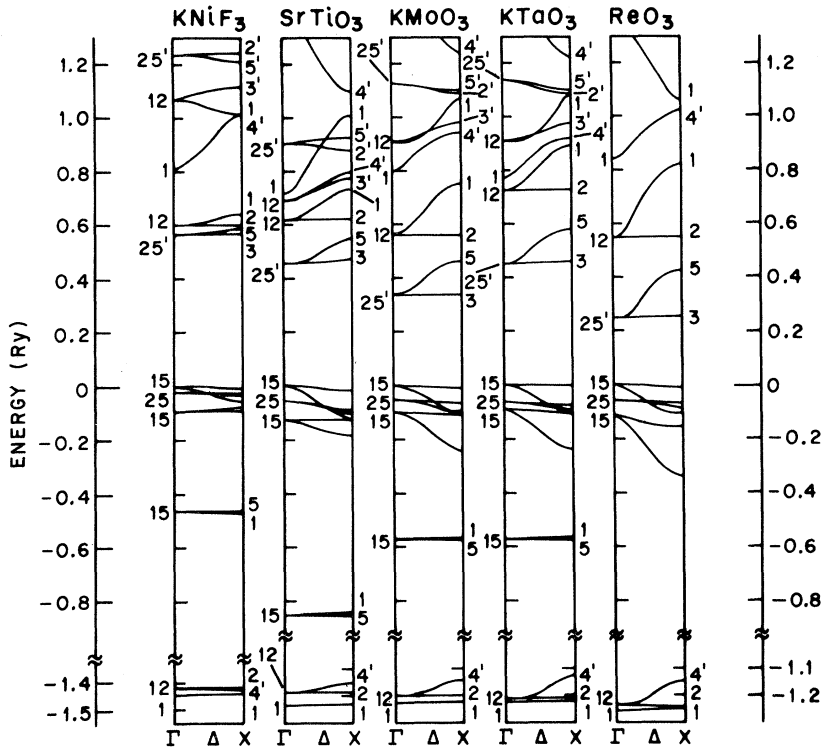

FIG. 2. APW results along the Δ line for several perovskite-type compounds and ReO_3. The energy scale to the lower left-hand side is for $KNiF_3$, the one to the lower right-hand side is for the oxide compounds.

gap. The dashed horizontal line in Fig. 5 is the Fermi energy for $K_{0.92}MoO_3$, assuming a rigid-band model with 0.92 electrons in the t_{2g} conduction bands. The Fermi energy for stoichiometric $KMoO_3$ would be raised by about 0.01 Ry.

The energy-band results for these perovskite-type compounds exhibit many similar features. In each case, a small energy gap separates the B-atom t_{2g} and e_g manifolds. According to Figs. 2–6, the relative energies of the antibonding s-p

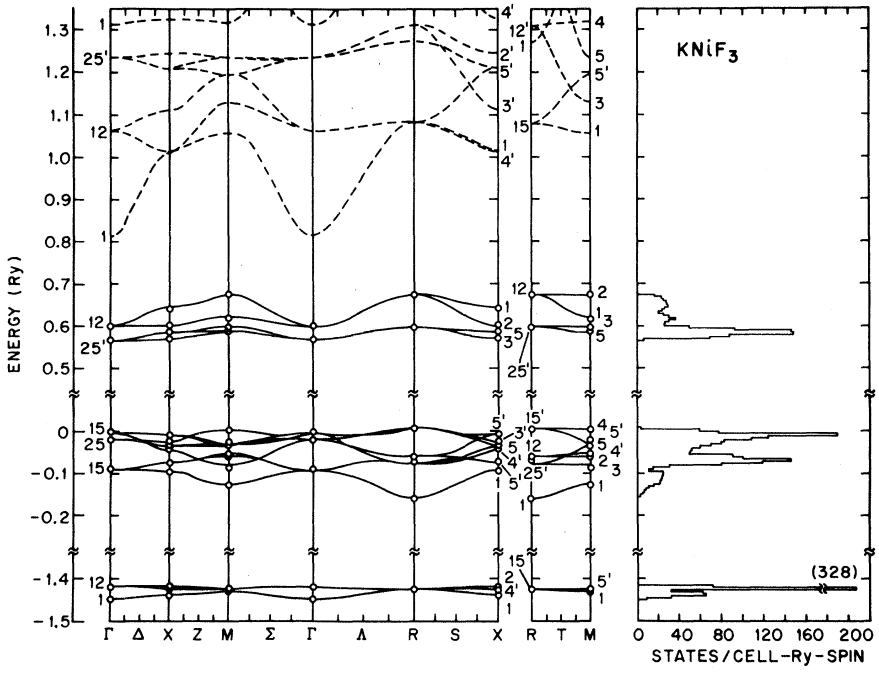

FIG. 3. LCAO band structure and density of states for $KNiF_3$ that is obtained by fitting APW results at symmetry points (open circles). The dashed lines represent higher conduction bands that are not included in this LCAO model.

TABLE V. APW results for perovskite-type compounds with formula ABC_3 (in rydbergs). The zero of energy has been shifted relative to the muffin-tin constant by an amount ΔE (the last entry) to set the energy of the highest Γ_{15} state equal to zero.

Band	State	$KNiF_3$	$SrTiO_3$	$KMoO_3$	$KTaO_3$	ReO_3
$C(2s)$	Γ_1	−1.4471	−1.2347	−1.2242	−1.2235	−1.2581
	Γ_{12}	−1.4195	−1.1859	−1.2003	−1.2102	−1.2348
	X_1	−1.4405	−1.2306	−1.2219	−1.2230	−1.2507
	X_2	−1.4172	−1.1834	−1.1975	−1.2076	−1.2390
	X_4'	−1.4242	−1.1589	−1.1434	−1.1311	−1.1499
	M_1	−1.4285	−1.2020	−1.2071	−1.2135	−1.2443
	M_5'	−1.4250	−1.1678	−1.1460	−1.1330	−1.1489
	R_{15}	−1.4250	−1.1591	−1.1437	−1.1320	−1.1468
$A(3p, 4p)$	Γ_{15}	−0.4659	−0.8568	−0.5734	−0.5712	···
	X_1	−0.4659	−0.8419	−0.5664	−0.5664	···
	X_5	−0.4628	−0.8535	−0.5700	−0.5685	···
	M_2'	−0.4601	−0.8497	−0.5647	−0.5642	···
	M_5'	−0.4703	−0.8546	−0.5763	−0.5744	···
	$R_{25'}$	−0.4756	−0.8733	−0.5925	−0.5874	···
$C(2p)$	Γ_{15}	0.0000	0.0000	0.0000	0.0000	0.0000
	Γ_{15}	−0.0875	−0.1262	−0.0974	−0.0899	−0.1181
	Γ_{25}	−0.0205	−0.0601	−0.0532	−0.0632	−0.0573
	X_1	−0.0933	−0.1853	−0.2438	−0.2297	−0.3392
	X_5	−0.0313	−0.0961	−0.1077	−0.1092	−0.1604
	X_3'	−0.0266	−0.0850	−0.0686	−0.0764	−0.0670
	X_4'	−0.0512	−0.1147	−0.0988	−0.1029	−0.1099
	X_5'	−0.0097	−0.0160	−0.0102	−0.0053	−0.0070
	X_5'	−0.0771	−0.1223	−0.0929	−0.0883	−0.0894
	M_1	−0.1268	−0.1998	−0.2235	−0.2078	−0.2868
	M_2	−0.0599	−0.1726	−0.2631	−0.2508	−0.3785
	M_3	−0.0879	−0.2158	−0.2223	−0.2148	−0.2811
	M_4	0.0051	−0.0065	−0.0003	−0.0154	0.0065
	M_5	−0.0379	−0.1174	−0.1224	−0.1215	−0.1571
	M_4'	−0.0550	−0.0510	−0.0307	−0.0144	−0.0248
	M_5'	−0.0209	−0.0661	−0.0561	−0.0648	−0.0772
	R_1	−0.1594	−0.2122	−0.1980	−0.1822	−0.2278
	R_{12}	−0.0610	−0.1732	−0.2641	−0.2518	−0.3811
	$R_{15'}$	0.0049	−0.0045	0.0005	−0.0150	0.0042
	$R_{25'}$	−0.0707	−0.1729	−0.1851	−0.1831	−0.2797
$B(3d,$ $4d, 5d)$	Γ_{12}	0.6009	0.6172	0.5596	0.7220	0.5440
	$\Gamma_{25'}$	0.5676	0.4576	0.3373	0.4526	0.2475
	X_1	0.6397	0.7339	0.7515	0.8882	0.8189
	X_2	0.6028	0.6205	0.5640	0.7293	0.5492
	X_3	0.5700	0.4715	0.3450	0.4639	0.2567
	X_5	0.5869	0.5482	0.4595	0.5793	0.4229
	M_1	0.6178	0.6688	0.6512	0.8080	0.6797
	M_2	0.6767	0.8294	0.8955	1.0641	1.0034
	M_3	0.5972	0.5952	0.5303	0.6636	0.5204
	M_5	0.5870	0.5476	0.4606	0.5797	0.4220
	R_{12}	0.6742	0.8254	0.8895	1.0606	0.9959
	$R_{25'}$	0.5972	0.5968	0.5303	0.6665	0.5144
$A(4d, 5d)$	Γ_{12}	1.0675	0.6889	0.9074	0.9115	···
	$\Gamma_{25'}$	1.2334	0.9029	1.1237	1.1325	···
	X_2'	1.2428	0.8781	1.0902	1.0842	···
	X_3'	1.1111	0.7713	0.9781	0.9737	···
	X_4'	1.0112	0.7929	0.9390	0.9169	···
	X_5'	1.2096	0.9231	1.1096	1.0996	···
	M_1	1.0585	0.8327	1.0192	1.0110	···
	M_3	1.1292	0.8394	1.0421	1.0315	···
	M_4	1.3200	1.0094	1.2156	1.2072	···
	M_5	1.2369	0.9467	1.1546	1.1561	···
	R_{15}	1.0818	0.7852	0.9694	0.9657	···
	$R_{12'}$	1.3105	0.9840	1.1961	1.1886	···
$A-B$ $(s-p)$	Γ_1	0.8146	0.7175	0.7986	0.7718	0.8461
	Γ_1	1.3135	···	1.5200	···	···
	X_1	1.0136	1.0040	1.0642	1.0739	1.06
	X_4'	1.3270	1.0941	1.2391	1.2223	1.02
	M_3	···	1.1500	1.2669	1.2545	···
	M_5'	1.1951	1.1008	···	···	···
	R_1	1.2716	···	1.4479	···	···
	ΔE	0.3430	−0.1168	−0.0660	−0.0500	0.1929

band and the potassium $3d$ bands are nearly constant for $KNiF_3$, $KMoO_3$, and $KTaO_3$, whereas the strontium $4d$ bands are shifted to slightly lower energies in $SrTiO_3$. These bands cross the titanium and tantalum e_g bands in $SrTiO_3$ and $KTaO_3$ and overlap the molybdenum e_g bands in $KMoO_3$. Nevertheless, this simplified LCAO model which neglects these antibonding s-p bands and the A-atom d bands seems to provide a rather accurate representation of the valence and lower conduction bands in these materials.

In addition to determining these energy-band curves, we have also applied this LCAO model to calculate some of the detailed electronic properties of these materials. These calculations include spin-orbit coupling for the B-atom d orbitals by means of a spin-orbit parameter ξ_{nd}. For simplicity, the individual values of ξ_{nd} for titanium, molybdenum, and tantalum were taken directly from the atomic calculations of Herman and Skillman,[18] where $\xi_{3d} = 0.0018$ Ry for titanium, $\xi_{4d} = 0.0074$ Ry for molybdenum, and $\xi_{5d} = 0.023$ Ry (estimated by interpolation) for tantalum.

Constant-energy surfaces in both the (100) and (110) planes for n-type $SrTiO_3$ and $KTaO_3$ are shown in Figs. 7(a) and 7(b), respectively, for a carrier density $n \approx 10^{19}$ cm^{-3}. It is found that the shapes of these constant-energy surfaces are quite similar, despite the differences in the t_{2g} bandwidths and the spin-orbit parameters for these materials. The conduction bands in n-type $SrTiO_3$ and $KTaO_3$ are analogous to the valence bands in p-type germanium and silicon.[21] In each class of materials, spin-orbit coupling splits the conduction-band minimum (valence-band maximum) into a lower (upper) fourfold degenerate Γ_8+ state and an upper (lower) doubly degenerate Γ_7+ state. The total splitting at Γ is about $\frac{3}{2}\xi_{nd}$ ($\frac{3}{2}\xi_{np}$) so that only the lower (upper) pair of bands are occupied at low temperatures in the lightly doped materials. Because of this similarity, it is appropriate to refer to the carriers associated with the inner and outer sheets in Fig. 7 as the "light" and "heavy" electrons, respectively.

The cross-sections of the $K_{0.92}MoO_3$ Fermi surface are shown in Fig. 8, where a rigid-band model is assumed with 0.92 electrons in the molybdenum t_{2g} bands. The three Fermi-surface sheets are labeled α, β, and γ, respectively. Their dimensions and shapes are quite similar to those obtained in the previous ReO_3 calculation.[13] The shaded regions designate the occupied portions of the third (α), second (β), and first (γ) bands. Both the α and β sheets are closed, while γ is open along the ⟨100⟩ directions. Detailed volume calculations predict that $n_\alpha = 0.097$, $n_\beta = 0.157$, and $n_\gamma = 0.670$ electrons/cell in $K_{0.92}MoO_3$. In ReO_3, the corresponding distribution of carriers was

TABLE VI. LCAO parameters for several compounds with the perovskite structure and ReO_3. Energies are in rydbergs.

Parameter	Two-center	$KNiF_3$	$SrTiO_3$	$KMoO_3$	$KTaO_3$	ReO_3
E_s	···	−1.4247	−1.1619	−1.1444	−1.1312	−1.1494
$(ss\sigma)$	···	−0.0030	−0.0098	−0.0103	−0.0118	−0.0135
$E_{p\sigma}$	···	−0.0579	−0.0597	−0.0401	−0.0238	−0.0393
$E_{p\pi}$	···	−0.0284	−0.0753	−0.0620	−0.0687	−0.0715
C_1	$\frac{1}{2}[(pp\sigma)_1+(pp\pi)_1]$	0.0075	0.0117	0.0087	0.0071	0.0095
C_2	$\frac{1}{2}[(pp\sigma)_1-(pp\pi)_1]$	0.0128	0.0196	0.0207	0.0213	0.0244
C_3	$\frac{1}{2}[(pp\sigma)_1-(pp\pi)_1]$	0.0085	0.0174	0.0155	0.0132	0.0202
C_4	$(pp\pi)_1$	−0.0024	−0.0028	−0.0025	−0.0021	−0.0043
$(pp\sigma)_2$	···	0.0011	0.0028	0.0027	0.0025	0.0041
$(pp\pi)_2$	···	−0.0007	−0.0016	−0.0019	−0.0023	−0.0019
E_d	···	0.5695	0.4663	0.3425	0.4584	0.2527
D_3	$(dd\delta)$	−0.0002	−0.0012	−0.0006	−0.0010	0.0002
D_6	$(dd\delta)$	−0.0001	−0.0001	−0.0004	−0.0026	−0.0007
$(sd\sigma)$	···	−0.0845	−0.1828	−0.2175	−0.2460	−0.2538
S_s	···	0.0282	0.0430	0.0504	0.0492	0.0543
$(pd\sigma)$	···	−0.0771	−0.1560	−0.1996	−0.2158	−0.2513
S_σ	···	0.0467	0.0777	0.0883	0.0925	0.0913
$(pd\pi)$	···	0.0378	0.0763	0.0887	0.0952	0.1117
S_π	···	−0.0183	−0.0584	−0.0684	−0.0722	−0.0730
RMS error		0.0034	0.0081	0.0068	0.0076	0.0043
Maximum error		0.0098	0.0221	0.0186	0.0228	0.0120

such that $n_\alpha = 0.093$, $n_\beta = 0.171$, and $n_\gamma = 0.736$ electrons/cell.

Extremal areas and cyclotron masses for orbits on these constant-energy surfaces have been calculated with this LCAO model using rather straightforward techniques.[13,22] The cyclotron-mass results for n-type $SrTiO_3$ and $KTaO_3$ are shown in Fig. 9 for carrier densities n in the 10^{18}–10^{19} cm^{-3} range. The masses for the light and heavy electrons are labeled α and β, respectively. Only one curve is shown for the light electrons, since these calculations show that the masses are independent of carrier density to within a percent or so. However, the results for the heavy electrons exhibit

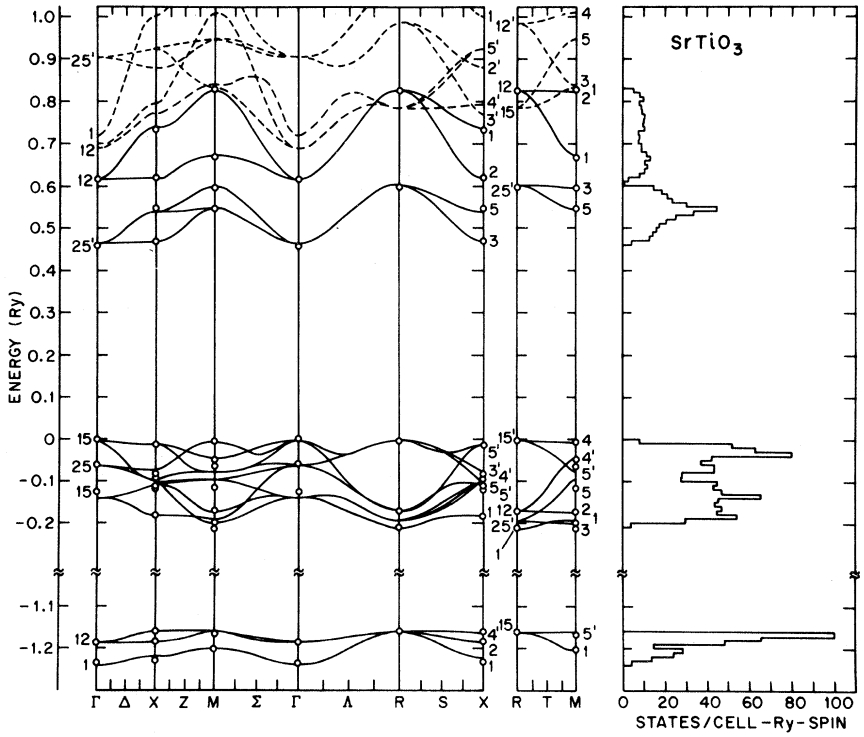

FIG. 4. LCAO band structure and density of states for $SrTiO_3$.

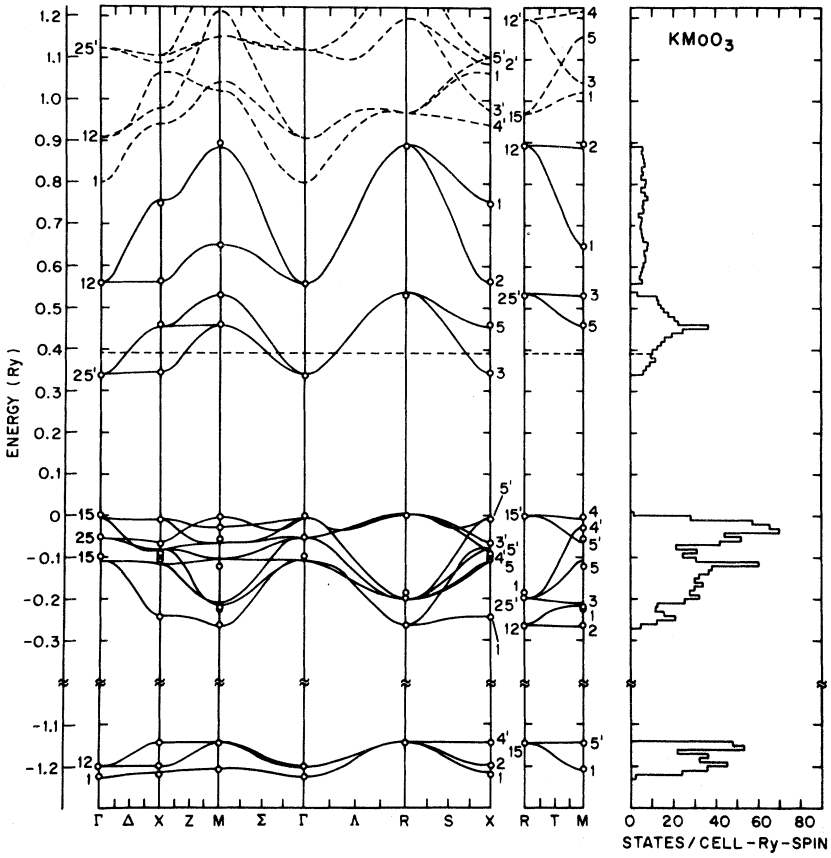

FIG. 5. LCAO band structure and density of states for $KMoO_3$.

a noticeable dependence on n, particularly for $SrTiO_3$. In Fig. 9, the curves labeled 1–3 correspond to the carrier densities which are listed in Table VII under the "fitted" heading. It is found that the cyclotron masses for the heavy electrons in $SrTiO_3$ can increase by as much as 33% for a tenfold increase in n, whereas the corresponding masses in $KTaO_3$ increase only by about 5%.

This dependence of the cyclotron mass on carrier density is caused by the nonparabolic nature of the

TABLE VII. LCAO density-of-states results for the fitted and adjusted $SrTiO_3$ and $KTaO_3$ band structures.

		Energy (Ry)	Carrier density (10^{18} cm^{-3})			State density (states/Ry spin cell)			
			n_α	n_β	n	N_α	N_β	N	m_D^*/m
					Fitted				
$SrTiO_3$	1	0.0001	0.249	0.598	0.847	0.113	0.271	0.384	2.40
	2	0.0003	1.302	3.297	4.599	0.195	0.524	0.719	2.47
	3	0.0005	2.814	7.560	10.374	0.253	0.744	0.997	2.55
$KTaO_3$	1	0.0002	0.328	0.826	1.154	0.079	0.199	0.278	1.48
	2	0.0006	1.714	4.351	6.065	0.136	0.350	0.486	1.49
	3	0.0010	3.698	9.470	13.168	0.177	0.459	0.636	1.49
					Adjusted				
$SrTiO_3$	1	0.0002	0.345	0.889	1.234	0.078	0.199	0.277	1.54
	2	0.0004	0.978	2.662	3.640	0.110	0.331	0.441	1.59
	3	0.0006	1.803	5.377	7.180	0.135	0.480	0.615	1.66
$KTaO_3$	1	0.0002	0.185	0.475	0.660	0.044	0.114	0.158	1.02
	2	0.0004	0.525	1.353	1.878	0.063	0.163	0.226	1.02
	3	0.0006	0.967	2.502	3.469	0.077	0.201	0.278	1.02

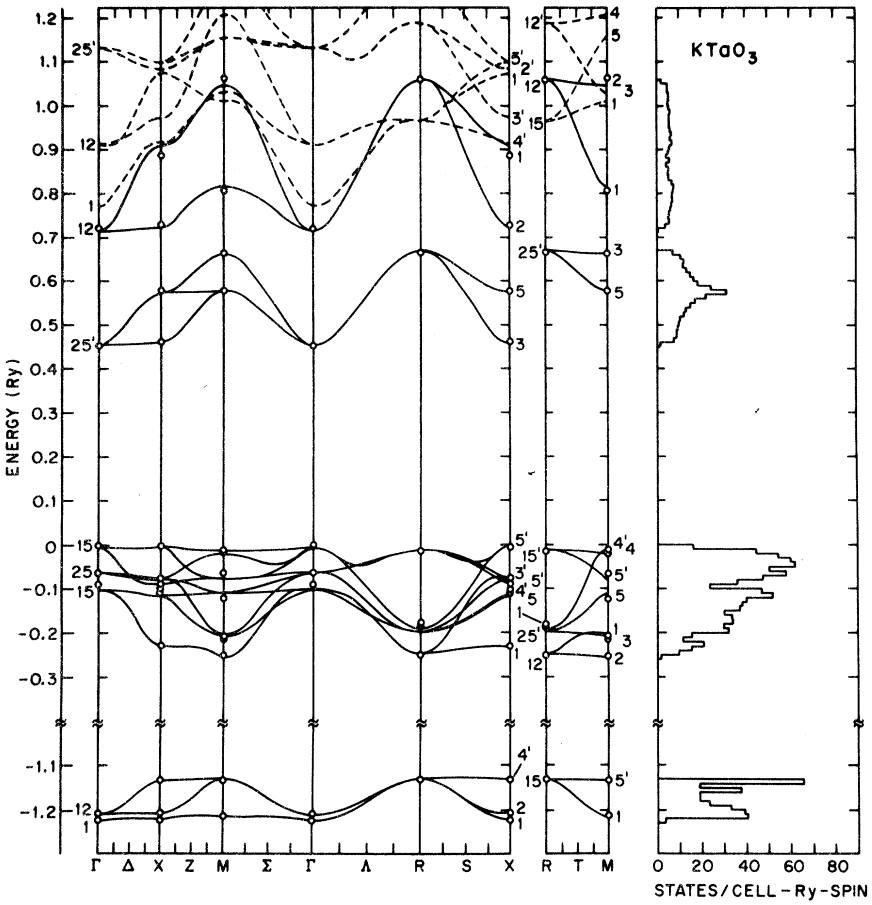

FIG. 6. LCAO band structure and density of states for $KTaO_3$.

bands along the Δ direction when $|\vec{k}| \gtrsim 0.05(\pi/a)$. The effect is more pronounced in $SrTiO_3$ because the spin-orbit parameter ξ_{3d} is comparable to the Fermi energy relative to the band edge. The magnitude of the mass variation for a particular orbit depends on the number of times it crosses these nonparabolic regions. Thus, the effect is largest for a central (100) orbit which crosses four Δ lines, intermediate for a (110) orbit which crosses only two, and quite small for a (111) orbit which avoids all these nonparabolic regions.

The fitted LCAO parameters of Table VI have been adjusted in accordance with the optical data for $SrTiO_3$ and $KTaO_3$ and the cyclotron-mass data for $K_{0.92}MoO_3$, as discussed in Sec. IV. The values for these adjusted LCAO parameters are listed in Table VIII. The adjustment procedure involves the modification of one parameter in each compound, the d-orbital energy E_d. However, a change in E_d also modifies the covalency parameters $(sd\sigma)$, $(pd\sigma)$, and $(pd\pi)$ when nonorthogonal orbitals are involved since these parameters contain a small term that is proportional to the product of E_d and the corresponding overlap integral.[14]

The adjusted LCAO band structures for $SrTiO_3$ and $KTaO_3$ are shown in Fig. 10. The main effect of the reduced p-d band gaps is to increase the valence and conduction bandwidths. The increased

TABLE VIII. Adjusted LCAO parameters for perovskite-type compounds.

Parameter	$SrTiO_3$	$KMoO_3$	$KTaO_3$	ReO_3
E_s	−1.1619	−1.1444	−1.1312	−1.1494
$(ss\sigma)$	−0.0098	−0.0103	−0.0118	−0.0135
$E_{p\sigma}$	−0.0597	−0.0401	−0.0238	−0.0393
$E_{p\pi}$	−0.0753	−0.0620	−0.0687	−0.0715
C_1	0.0117	0.0087	0.0071	0.0095
C_2	0.0196	0.0207	0.0213	0.0244
C_3	0.0174	0.0155	0.0132	0.0202
C_4	−0.0028	−0.0025	−0.0021	−0.0043
$(pp\sigma)_2$	0.0028	0.0027	0.0025	0.0041
$(pp\pi)_2$	−0.0016	−0.0019	−0.0023	−0.0019
E_d	0.2200	0.2425	0.2584	0.0527
D_3	−0.0012	−0.0006	−0.0010	0.0002
D_6	−0.0001	−0.0004	−0.0026	−0.0007
$(sd\sigma)$	−0.1881	−0.2200	−0.2510	−0.2592
S_s	0.0430	0.0504	0.0492	0.0543
$(pd\sigma)$	−0.1656	−0.2040	−0.2250	−0.2604
S_σ	0.0777	0.0883	0.0925	0.0913
$(pd\pi)$	0.0835	0.0921	0.1025	0.1190
S_π	−0.0584	−0.0684	−0.0722	−0.0730

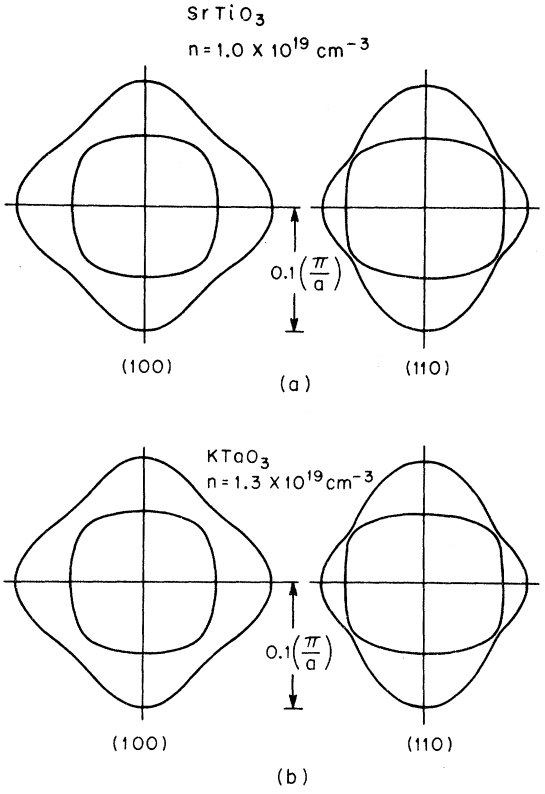

FIG. 7. Constant-energy surfaces in the (100) and (110) planes for n-type $SrTiO_3$ and $KTaO_3$. These correspond to the third and sixth entries in Table VII.

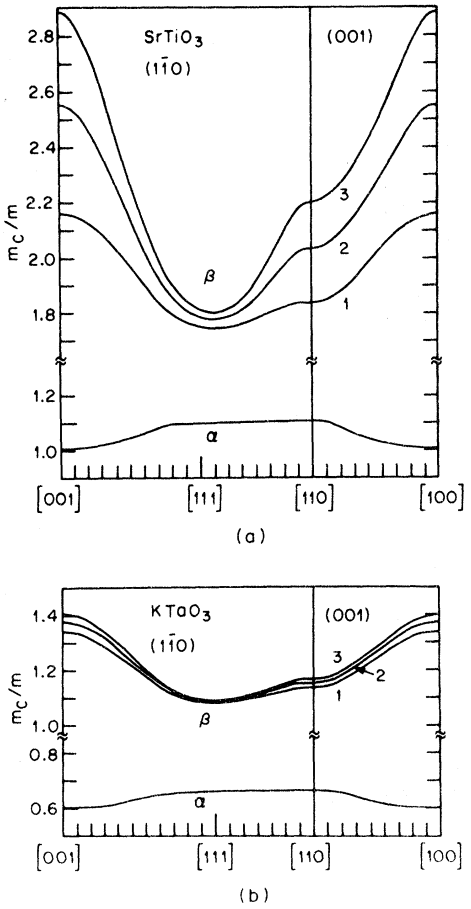

FIG. 9. Cyclotron masses for orbits on the $SrTiO_3$ and $KTaO_3$ constant-energy surfaces as a function of angle. The curves labeled 1–3 correspond to the carrier densities which are listed in Table VII under "Fitted."

conduction bandwidth is reflected in the cyclotron-mass results that are derived from the adjusted LCAO band structures for $SrTiO_3$ and $KTaO_3$, as shown in Fig. 11. A comparison between the fitted cyclotron masses of Fig. 9 and the adjusted masses of Fig. 11 indicates that the latter are reduced by about 40%. However, the angular variation of the masses is quite similar in both cases. The mass of the heavy electrons again depends on the carrier density. The curves labeled 1–3 in Fig. 11 correspond to the carrier densities that are listed in Table VII under the "adjusted" heading.

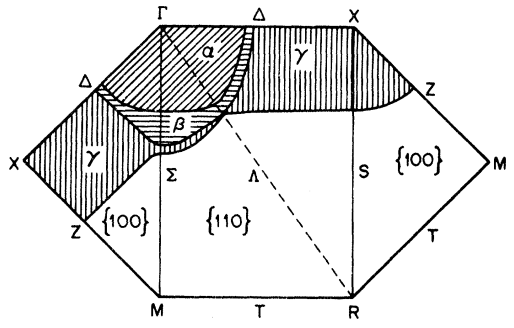

FIG. 8. Central {110} and {100} cross sections of the $K_{0.92}MoO_3$ Fermi surface.

IV. COMPARISON WITH EXPERIMENT

A. $KNiF_3$

Potassium nickel fluoride is one of a series of perovskite-type antiferromagnetic insulators which includes $KMnF_3$, $KFeF_3$, $KCoF_3$, and $KCuF_3$. Each of these crystals is transparent and their respective colors vary from light brown to brown, rose, yellow-green, and finally pale violet.[23] Within this group of antiferromagnetic insulators, $KNiF_3$ is unique in that it appears to remain cubic below its Néel temperature, whereas the others become either monoclinic, rhombohedral, or tetragonal at low temperatures.[23]

Optical studies provide the most useful information concerning the electronic structure of $KNiF_3$. The results of numerous measurements demonstrate rather convincingly that the proper descrip-

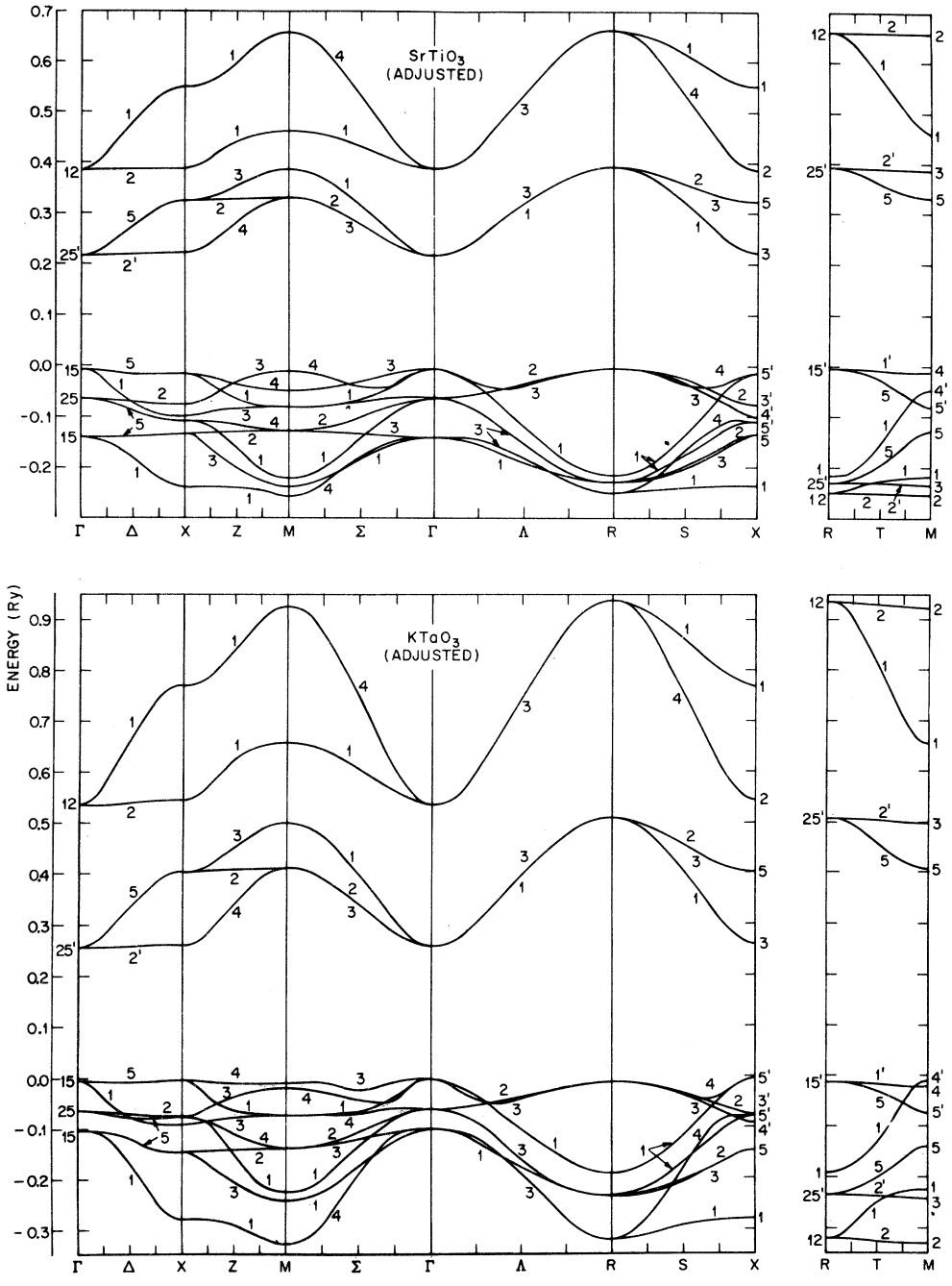

FIG. 10. Adjusted LCAO band structures for $SrTiO_3$ and $KTaO_3$.

tion of the ground and low-lying excited states in $KNiF_3$ (as well as the other fluoride compounds) requires the ligand-field theory of d-electron multiplets in crystals[24] rather than one-electron band theory. A similar conclusion has been reached in the case of the $3d$ monoxides MnO through NiO,[16,25] which are also antiferromagnetic insulators with very similar optical properties.

The most interesting result of these optical studies is the fact that the low-energy spectra are remarkably similar for a wide variety of compounds which contain nickel ions in a perfect or slightly distorted octahedral environment of nearest-neighbor fluorine ions. For example, the reflectivity measurements by Rüdorff *et al.*[26] on $KNiF_3$, NiF_2, K_2NiF_4, Rb_2NiF_4, Li_2NiF_4, and $NaNiF_3$ yield peaks in the reflectivity at photon energies of 1.6, 1.9, 2.6, and 3.0 eV which shift by less than ± 0.1 eV

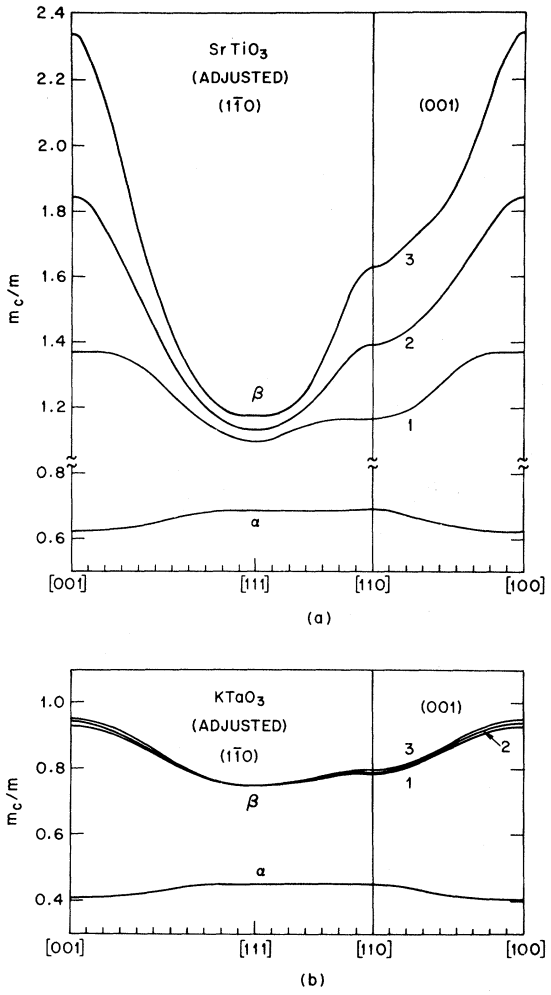

FIG. 11. Cyclotron masses derived from the adjusted LCAO band structures for $SrTiO_3$ and $KTaO_3$ as a function of angle. The curves labeled 1–3 correspond to the carrier densities which are listed in Table VII under "Adjusted."

from one compound to another. Furthermore, the energies of these peaks are within ± 0.3 eV of those that are observed in the absorption spectra of nickel substituted in[27] MgO and pure NiO.[28] Subsequent measurements by Knox *et al.*[29] on pure $KNiF_3$ and nickel substituted in $KMgF_3$ were extended to lower photon energies and revealed an additional absorption peak at 0.9 eV. They showed that the positions of all five absorption bands could be fitted accurately within the ligand-field theory by means of three parameters, including a crystal field parameter $\Delta = 0.90$ eV and two Racah parameters,[24] $A = 0.12$ eV and $B = 0.52$ eV. More recent studies on pure NiF_2[30] and $KNiF_3$[31] and samples containing dilute traces of nickel in $KMgF_3$,[31,32] $KZnF_3$,[32] MgF_2,[33] and ZnF_2[33] have produced essentially the same spectra.

As in the case of the 3*d* monoxides,[16] this similarity in the absorption spectra for dilute and concentrated nickel-fluoride compounds is difficult to understand unless one assumes that the nickel 3*d* electrons in the latter compounds exist in localized-Wannier rather than itinerant-Bloch states, presumably because the nickel 3*d* bandwidths are small compared to U, the Coulomb repulsion energy between two d electrons on the same atom. In this localized limit, the e_g and t_{2g} Wannier functions have one-electron energies that correspond to the average energies of the e_g and t_{2g} bands, respectively, and the 3*d* bandwidth produces the antiferromagnetic exchange coupling between localized spins on neighboring ions.[14] On expects a similarity between these Wannier functions in the stoichiometric compounds and the localized 3*d* impurity wave functions in the dilute systems, since both are expected to fall off quite rapidly beyond the nearest shell of neighboring fluorines. Essentially, the MO calculations that approximate the $KNiF_3$ crystal by a single $(NiF_6)^{4-}$ octahedral complex[7] are based on the implicit assumption that the nickel 3*d* electrons are localized rather than itinerant.

The first successful attempt to calculate the crystal field parameter Δ for $KNiF_3$ was the MO calculation for the $(NiF_6)^{4-}$ complex by Sugano and Shulman.[34] We have previously applied their MO integrals to determine the LCAO band structure for $KNiF_3$ (see Fig. 5 of Ref. 14). In the case of the perovskite structure, the average e_g and t_{2g} band energies are given by

$$\langle e_g \rangle = \tfrac{1}{2}[E(\Gamma_{12}) + E(R_{12})] , \tag{1}$$

$$\langle t_{2g} \rangle = \tfrac{1}{2}[E(\Gamma_{25'}) + E(R_{25'})] , \tag{2}$$

so that $\Delta \equiv \langle e_g \rangle - \langle t_{2g} \rangle$ is easily determined from the present energy-band results. The MO integrals of Sugano and Shulman predict that $\Delta = 0.69$ eV, whereas the present APW results of Table V predict that $\Delta = 0.75$ eV. These values are 20–25% smaller than the experimental value of 0.90 eV.

One advantage of the present energy-band approach over the MO method is that it provides realistic estimates of the positions of higher-energy conduction bands. In $KNiF_3$, absorption measurements have been extended to photon energies as high as 6.2 eV[35] with no indication of an absorption edge. This is in contrast to the situation in the 3*d* monoxides, where Powell and Spicer[36] observe an edge at 3.7 eV in both MnO and NiO. They have tentatively interpreted this edge in terms of transitions from localized 3*d* orbitals to antibonding *s-p* bands. The absence of such an edge in $KNiF_3$ below 6 eV suggests that the position of the nickel 3*d* bands is lower by several electron volts from that shown in Fig. 3, where

an absorption edge is predicted near 3 eV. An adjusted LCAO calculation for $KNiF_3$ in which the energy of the nickel $3d$ bands is lowered by 0.2 Ry produces a $3d$ bandwidth that is 25% greater than that shown in Fig. 3. This adjustment also increases the crystal field parameter Δ to 0.85 eV, which is in better agreement with experiment.

B. $KMoO_3$

The nonstoichiometric compounds K_xMoO_3 and Na_xMoO_3 are two examples of an interesting class of ternary compounds known as the "bronzes."[37] These materials are usually good conductors and they form with different crystal structures in different ranges of x. The best known examples are the tungsten bronzes, which normally have the perovskite structure when x is close to 1.

Under ordinary conditions, the molybdenum bronzes do not form with the perovskite structure. However, Bither *et al.*[38] have shown that cubic samples of $Na_{0.90-0.97}MoO_3$ and $K_{0.89-0.93}MoO_3$ are obtained if the material is heated to 400–1000 °C under pressures of about 65 kbar. These crystals have a bright red color, a metallic luster, and low-temperature resistivities in the 10^{-6}-Ω cm range.

Marcus and Bither[10] have observed de Haas–van Alphen oscillations in $Na_{0.93}MoO_3$ and $K_{0.92}MoO_3$ samples. Both the range of frequencies and their variation with magnetic field direction $\vec{H}$ in the (100) and (110) planes are very similar to those observed previously in ReO_3.[11,12] One new feature of the $Na_{0.93}MoO_3$ data is the existence of a low-frequency branch with oscillations that are 50–100 times slower than the main branches of $Na_{0.93}MoO_3$, $K_{0.92}MoO_3$, and ReO_3. Marcus and Bither find that this branch does not possess cubic symmetry, though they find no x-ray evidence for a noncubic distortion at 4.2 °K.

The fitted LCAO parameters of Table VI have been applied to calculate extremal cross-sectional areas and cyclotron masses for orbits on the $K_{0.92}MoO_3$ Fermi surface, assuming a rigid-band model with 0.92 electrons in the molybdenum t_{2g} bands and a spin-orbit parameter $\xi_{4d} = 0.0074$ Ry. The results are shown in Fig. 12(a), where the solid lines are the calculated extremal areas and the open circles are the experimental results. The branches labeled α, β, and γ correspond to orbits on the three Fermi-surface sheets that are shown in Fig. 8. The areas labeled γ_1 represent orbits on the nearly cylindrical arms of the open γ sheet which are centered at X, on the surface of the Brillouin zone.

The over-all agreement between the calculated and experimental areas in Fig. 12(a) is rather good, considering that these calculations involve no adjustable parameters. The maximum error is about 20%. It is shown in Fig. 12(b) that a slightly improved fit to the experimental data can be achieved if the Fermi energy is raised by 0.0025 Ry. Within this rigid-band model, these results correspond to $K_{0.98}MoO_3$ rather than $K_{0.92}MoO_3$. This shift in the Fermi energy reduces the maximum error to about 10%.

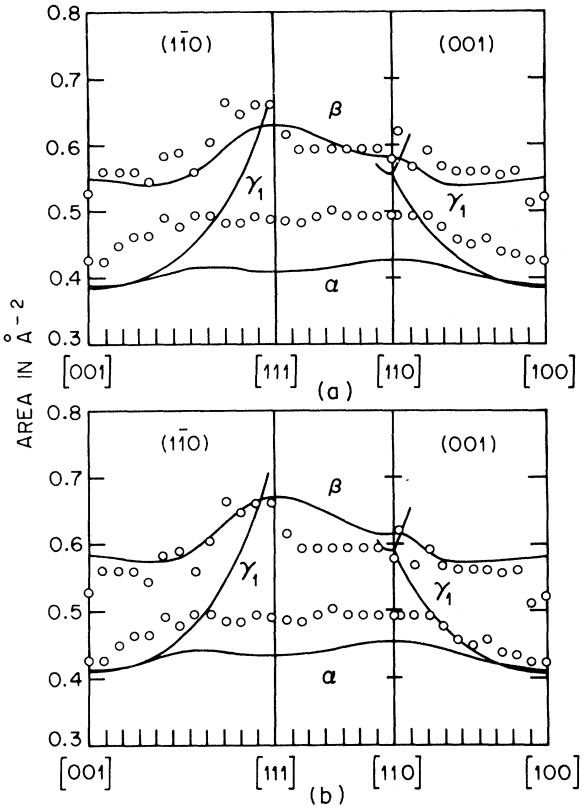

FIG. 12. Comparison between the de Haas–van Alphen results of Marcus and Bither (open circles) and the calculated extremal areas for K_xMoO_3, with (a) $x = 0.92$ and (b) $x = 0.98$.

Marcus and Bither have measured the cyclotron mass for the α orbit with $\vec{H}$ along [100] and find that $m_c/m = 0.78$. The calculated value for this mass ratio is 0.89. Similar calculations for the β and γ_1 orbits yield mass ratios of 1.18 and 0.83, respectively. Although this cyclotron-mass data is quite limited, we tentatively attribute this discrepancy between the calculated and experimental mass ratios to an inaccuracy in the calculated $2p$-$4d$ band gap. The adjusted LCAO parameters for $KMoO_3$ in Table VIII involve a $2p$-$4d$ band gap which is reduced by 0.1 Ry.

The areas and cyclotron masses for K_xMoO_3 have been calculated using these adjusted LCAO parameters. In these calculations, we have also varied the spin-orbit parameter ξ_{4d} because the relative areas enclosed by the α and β orbits are

sensitive functions of this parameter.[13] The best fit to the experimental data is obtained with $\xi_{4d} = 0$ and $x = 0.97$. The Fermi-surface cross sections for $K_{0.97}MoO_3$ with $\xi_{4d} = 0$ are shown in Fig. 13(a) and the calculated and experimental areas are compared in Fig. 13(b). The calculated cyclotron-mass ratios for the α, β, and γ_1 orbits are reduced to 0.79, 1.06, and 0.76, respectively. The density of states at the Fermi level for the adjusted K_xMoO_3 band structure is 9.79 states/(Ry spin cell), as compared to the value of 10.66 states/(Ry spin cell) that is derived from the fitted K_xMoO_3 band structure.

Although we have not attempted a similar calculation for Na_xMoO_3, it seems likely that similar accuracy can be achieved in fitting the de Haas–van Alphen data for this compound. The present LCAO results for $KMoO_3$ suggest a possible explanation for the low-frequency oscillations that are observed in $Na_{0.93}MoO_3$. According to the results of Figs. 12 and 13, the areas of the α and γ_1 branches are nearly equal in K_xMoO_3 when $\vec{H}$ is along [100]. It is also found that these orbits have similar cyclotron masses. This combination of similar areas and masses could produce a strong

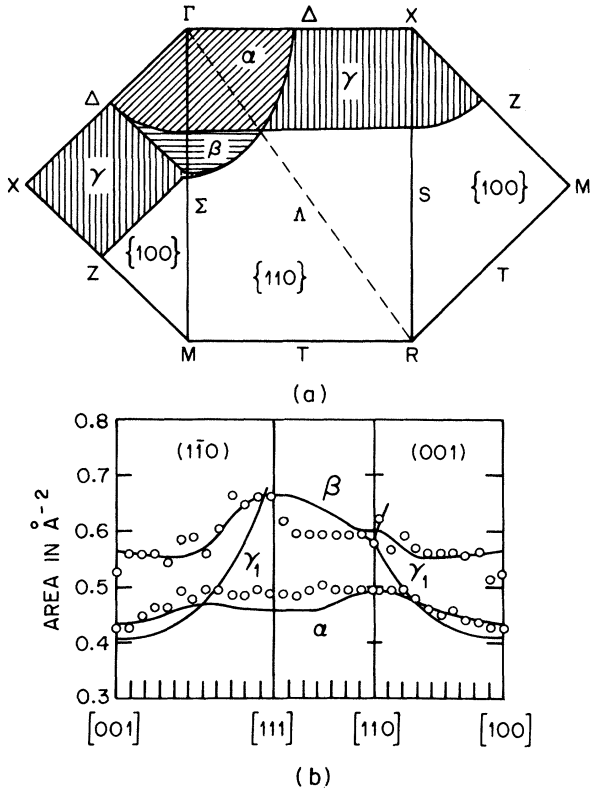

FIG. 13. Calculated Fermi-surface cross sections and extremal areas which are derived from the adjusted LCAO band structure for K_xMoO_3, with $x = 0.97$ and $\xi_{3d} = 0$.

difference frequency, which might account for the observed low-frequency oscillations in $Na_{0.93}MoO_3$. This explanation is particularly attractive since the angular variation of this low-frequency branch in a (100) plane is quite similar to that expected for the difference in the α and γ_1 extremal areas in K_xMoO_3, particularly in Fig. 12, where α and γ_1 are nearly degenerate when $\vec{H}$ is along [100]. However, in view of the inherent instability of the perovskite-type compounds, one cannot rule out the possibility that this low-frequency branch in Na_xMoO_3 is caused by a low-temperature structural transformation.

It is well known that the observation of the de Haas–van Alphen effect normally requires pure stoichiometric single-crystal samples. The present APW results for $KMoO_3$ in Fig. 5 suggest a possible explanation for the fact that this effect is observed in grossly nonstoichiometric Na_xMoO_3 and K_xMoO_3 samples. They suggest that the electronic states at the K_xMoO_3 Fermi energy consist essentially of molybdenum-t_{2g} states, with some (antibonding) admixture of oxygen-$2p$ orbitals. According to this model, the conduction electrons are confined to the molybdenum and oxygen sites, and therefore are not scattered by vacancies at the sodium or potassium sites.

C. $SrTiO_3$ and $KTaO_3$

There has been an extensive experimental effort to determine the electronic properties of $SrTiO_3$ and $KTaO_3$ since the KL band-structure model for $SrTiO_3$ was proposed.[3] Frederikse and co-workers[39,40] have reviewed the experimental evidence concerning the nature and symmetry of the $SrTiO_3$ conduction bands. They find that the bulk of this evidence strongly favors the KL model for the $SrTiO_3$ conduction bands with energy minima located at or near the Brillouin-zone boundaries in the ⟨100⟩ directions; however, they also note that this evidence does not rule out a model involving warped bands at the zone center.[40]

Stoichiometric samples of $SrTiO_3$ and $KTaO_3$ are colorless and transparent. The best samples have resistivities greater than 10^{10} Ω cm.[41,42] Slightly reduced or doped samples acquire a light-blue color, which becomes darker as the carrier density is increased. The low-temperature resistivities of the more heavily doped samples are as small as 10^{-4} Ω cm. Thus far, all measurements have involved n-type samples since it has not been possible to prepare p-type samples of either compound.

Cubic $SrTiO_3$ distorts to a tetragonal structure at about 110 °K, and there are some indications that additional phase transitions may occur at 65 and 10 °K.[8] There have been reports of noncubic distortions in $KTaO_3$, but it is believed that these

are due to growth-related strains rather than a structural transformation.[42] The present discussion is concerned primarily with the interpretation of the experimental data for cubic $SrTiO_3$ and $KTaO_3$. A more detailed consideration of the low-temperature data for $SrTiO_3$ is reserved for the following paper,[17] where we consider the effect of the cubic-to-tetragonal structural transformation on the $SrTiO_3$ conduction bands.

We consider first the optical data for $SrTiO_3$ and $KTaO_3$, since these results have been involved in the determination of the adjusted LCAO parameters of Table VIII. Cardona[43] and Kurtz[44,45] have measured the ultraviolet reflectance spectra of $SrTiO_3$ and $KTaO_3$, respectively, and have applied standard Kramers-Kronig procedures to determine the real and imaginary parts of the dielectric constant (ϵ_1 and ϵ_2) for these materials. In Fig. 14 we compare the density-of-states (DS) and joint-density-of-states (JDS) curves for the adjusted $SrTiO_3$ and $KTaO_3$ band structures of Fig. 10. These curves are obtained by sampling 64 000 uniformly distributed points in the Brillouin zone. They have been smoothed by averaging the results over three successive energy intervals, using a method described by Brust.[46]

In the lower portion of Fig. 14 we compare the $\epsilon_2(\omega)$ curves of Cardona and Kurtz with JDS/ω^2, which is proportional to $\epsilon_2(\omega)$ if the interband matrix elements are constant.[46] It is found that this simplified model provides a qualitative interpretation of the structure in the ϵ_2 curves below 8 eV. Although there are some differences in the shapes of the ϵ_2 and JDS/ω^2 curves, the positions of the various peaks and shoulders tend to line up quite well. There is some evidence that surface effects may alter the shapes of the experimental ϵ_2 curves in these materials. In similar measurements on $BaTiO_3$ samples, Cardona[43] finds that the relative intensities of the two lowest-energy reflectivity peaks changes if as-grown surfaces are substituted for polished and etched surfaces. Cardona's reflectivity measurements on $SrTiO_3$ involved polished and etched surfaces, whereas Kurtz used natural growth faces for his $KTaO_3$ measurements. It is possible that this may account for the difference in shape of the lowest-energy peak in the ϵ_2 curves for $SrTiO_3$ and $KTaO_3$.

We have not attempted a detailed interpretation of the additional structure in the ϵ_2 curves above 8 eV since this includes the energy range where transitions to the antibonding s-p bands and the A-atom d bands are expected to commence. In the lower portion of Fig. 14, we indicate the positions of

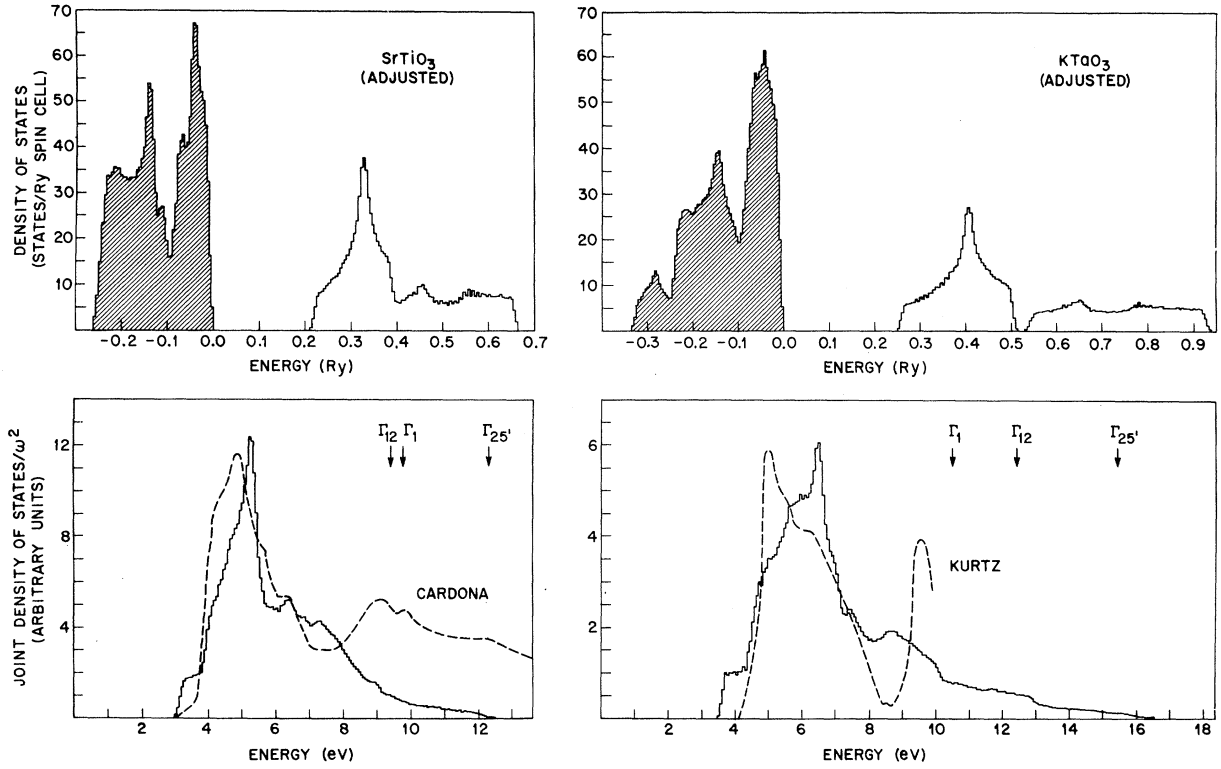

FIG. 14. DS and JDS curves for the adjusted LCAO band-structure models for $SrTiO_3$ and $KTaO_3$ and a comparison with the experimental ϵ_2 (dashed) curves.

the bottom of the antibonding s-p band (Γ_1) and the A-atom d states at $\Gamma(\Gamma_{12}$ and $\Gamma_{25'})$, as predicted by the APW calculations. In view of the adjustments that are required in the APW-LCAO results to fit the observed p-d band gaps in these materials, the energies of these states could easily be in error by several electron volts.

A similar interpretation of the optical data for ReO_3 is shown in Fig. 15. Here, we compare the ϵ_2 curve of Feinleib *et al.*[47] with the JDS/ω^2 curve for the adjusted ReO_3 band structure. Again, there is close agreement between the two curves below 8 eV and the additional structure at higher energies probably involves the antibonding s-p bands as final states.

There have been numerous attempts to determine accurate values for the band gaps in both $SrTiO_3$[43,48,49] and $KTaO_3$.[42,45,49,50] However, the absorption threshold is obscured by the occurrence of Urbach tails in these materials. The most recent studies on $SrTiO_3$ samples by Capizzi and Frova[48(e)] and Blazey[48(f)] suggest an indirect gap at 3.3 eV and a direct gap at 3.4 eV. Frova and Boddy[50(a)] interpret their electroreflectance data on $KTaO_3$ in terms of a 3.6-eV indirect edge and a 4.4-eV direct gap.

The present APW calculations for $SrTiO_3$ and $KTaO_3$ predict that the fundamental p-d band gaps are direct in both compounds, with valence-band maxima and conduction-band minima at the zone center. However, it is noted that the position of the valence-band maximum shifts to M in $KNiF_3$ and ReO_3 and to R in $KMoO_3$. In each material, energy differences of about 0.005 Ry separate one or more states from the valence-band maximum. Thus, it is believed that self-consistency effects or an improved treatment of exchange and correlation could easily shift the calculated position of the valence-band maximum in either $SrTiO_3$ or $KTaO_3$. These results do suggest that the difference between the direct and indirect gaps in both materials is probably about 0.1 eV.

Tredgold and Williams[51] and Derbenwick[52] have carried out photoemission studies on $SrTiO_3$ samples. Although they obtain similar results, they disagree in their interpretation, particularly on the position of the vacuum level relative to the top of the valence bands. Tredgold and Williams suggest that the vacuum level is 4.5 eV above the valence band whereas Derbenwick places it at 6.7 eV. Derbenwick's attempt to lower the vacuum level by cesiation produced unsatisfactory results. Consequently, these studies provide little information about transitions from the oxygen $2p$ to the lower portions of the titanium $3d$ conduction bands. Derbenwick estimates from his data that the ox-

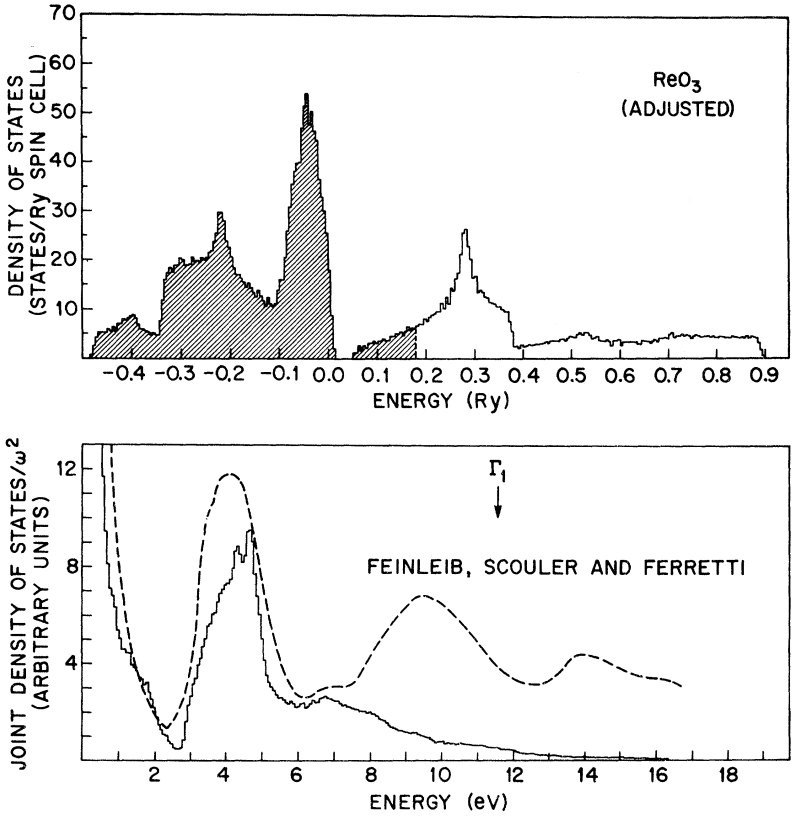

FIG. 15. Adjusted LCAO results for ReO_3 comparing the calculated JDS and experimental ϵ_2 curves.

ygen $2p$ bandwidth is between 5 and 6 eV. X-ray emission studies suggest a 3.6-eV bandwidth in $SrTiO_3$.[53] This is in good agreement with the adjusted LCAO band structure for $SrTiO_3$ which, according to Fig. 14, predicts a $2p$ bandwidth of 0.26 Ry or 3.5 eV.

A variety of experiments have been performed to measure the effective masses for the conduction electrons in n-type $SrTiO_3$ and $KTaO_3$. These results are summarized in Table IX, where the results are listed in approximately chronological order. It should be noted that these masses are not all equivalent, since they include DS masses, cyclotron masses, and mobility masses. In addition, their determination often depended on the assumption of a particular model for the conduction bands, usually the KL many-valley model.

Nevertheless, the results of Table IX show that a wide range of masses are observed in these materials, particularly in $SrTiO_3$. Typically, $m^*/m \approx 5$ in $SrTiO_3$ and 0.6 in $KTaO_3$. For comparison, we have estimated the DS masses for $SrTiO_3$ and $KTaO_3$ using the results of Table VII and the simplified formula

$$E_f = (\hbar^2/2m_D^*)\,(3\pi^2 n)^{2/3} \quad . \tag{3}$$

The results are contained in the last column of Table VII for both the fitted and adjusted LCAO models. In general, the calculated masses for $SrTiO_3$ are smaller than the experimental values while those for $KTaO_3$ tend to be somewhat larger.

The results of the recent cyclotron-resonance studies by Walsh *et al.*[63] provide some support for the present warped-band model for n-type $KTaO_3$. With the magnetic field along [100], they observe absorption peaks which correspond to two distinct carriers with m_c/m equal to 0.6 and 1.4, respectively. We associate these with the light and heavy electrons. According to the results of Fig. 11, this implies an enhancement factor of about 1.5 for both sets of carriers. One significant feature of these data is the occurrence of harmonic resonances for the heavy electrons at lower magnetic fields. These are a unique characteristic of warped energy surfaces and they have been observed previously for the heavy holes in both p-type germanium and silicon.[64] These resonances are also present in the low-field data of Senhouse *et al.*,[54] but they did not extend their measurements to high enough magnetic fields to observe the fundamental heavy-electron absorption peak.

In principle, the Shubnikov–de Haas effect[59] could distinguish between the many-valley and warped-band models for n-type $SrTiO_3$. However, this would require monodomain samples, since the results of the following paper[17] predict that the cubic-to-tetragonal structural transformation produces significant changes in the $SrTiO_3$ conduction bands. Frederikse *et al.*[59] assume parabolic bands and interpret their Shubnikov–de Haas frequencies in terms of cyclotron masses. The present calculations suggest that this assumption is invalid, at least for the carrier densities that they infer from their Hall measurements.

Eagles[65] has suggested an explantion for the fact that the effective masses for $SrTiO_3$ which are determined from Šroubek's tunneling data[61] are significantly smaller then the heat capacity[56,60] and magnetic susceptibility[55] results. He proposes that the carriers in bulk $SrTiO_3$ consist of equal numbers of large and small polarons. He suggests that the electric fields in the junction region switch all the tunneling electrons into the large-polaron regime. However, Phillips *et al.*[60] note that the values which they quote for the electronic contributions to the heat capacity γ must be regarded as uncertain. They find that their heat-capacity data for $SrTiO_3$ do not exhibit the temperature dependence that is expected for the sum of lattice and electronic contributions to the heat capacity. They find additional contributions from paramagnetic centers and possibly a term from the low-temperature structural transformations. It is possible that these effects are responsible for the apparent discrepancy between the heat capacity and tunneling values for the DS effective mass in $SrTiO_3$.

Low-field magnetoresistance measurements have been performed on $SrTiO_3$[66,67] and $KTaO_3$[68,69] to determine the symmetry of the conduction bands. These results are consistent with a many-valley model with ellipsoids at X or a warped-band model at the zone center. Although Mavroides and Lax[70] have worked out the theory for calculating the low-field magnetoresistance anisotropy for warped bands, the application of this theory requires a detailed knowledge of the scattering relaxation times for the various sheets and their anisotropies, and these are not well understood at the present time.

TABLE IX. Summary of experimental values for effective masses in n-type $SrTiO_3$ and $KTaO_3$.

Experiment	n (10^{18} cm^{-3})	T (°K)	$SrTiO_3$ m^*/m	$KTaO_3$ m^*/m	Ref.
Hall–Seebeck	1–12	300	14	···	41
Hall–Seebeck	1–12	78	6	···	41
Hall–Seebeck	0.4	300	···	0.8	42
Cyclotron resonance	0.2	1.4	···	0.2–0.6	54
Magnetic sus.	75–530	4.2	5.0	···	55
Heat capacity	140	0.5	5.3	···	56
Reflectivity	500	300	2.8	···	57
Reflectivity	500	90	1.1	···	57
Faraday rotation	1.8	300	···	0.42	58
Shubnikov–de Haas	5–6	1.4–4.2	2,3,3.5	···	59
Heat capacity	30–120	0.7–6.0	5.1–7.8	···	60
Tunneling	7–50	4.2	1.3	···	61
Tunneling	8	4.2	···	0.7	61
Tunneling	8	4.2	···	0.5	62
Cyclotron resonance	0.7	1.4	···	0.6,1.4	63

Tufte and Stelzer[71] and Frederikse *et al.*[72] have measured the piezoresistive properties of *n*-type $SrTiO_3$ in the temperature range from 4.2 °K to room temperature. On the basis of their room-temperature results, Tuft and Stelzer conclude that the conduction-band minimum in cubic $SrTiO_3$ occurs at the zone center and that the constant-energy surfaces are spherical. They also suggest the presence of a second extremum that is 0.02–0.04 eV above this minimum. This may correspond to the Γ_7+ state, which is raised above the Γ_8+ conduction-band minimum by 0.038 eV when $\xi_{3d}=0.0018$ Ry. At low-temperatures, the piezoresistance effects are large and anisotropic. They appear to be caused by the stress-induced alignment of domains in tetragonal $SrTiO_3$. These low-temperature data are considered in the following paper.

V. DISCUSSION

Goodenough[73] has surveyed the more than fifty known ABO_3 oxides (excluding the rare-earth oxides) with the perovskite structure. He separates these compounds into two types by means of a phenomenological parameter b, which measures the interactions between d electrons on nearest-neighbor atoms. The d electrons in those materials for which b is greater than a critical value b_c can be described in terms of collective band-type states; in those systems where $b<b_c$, the d electrons form localized states. The localized systems include ABO_3 oxides in which the B atoms are either vanadium, chromium, manganese, or iron.

More than twenty of these ABO_3 oxide compounds (including $SrTiO_3$ and $KTaO_3$) are insulators with p-d band gaps in the 2.5–3.5 eV range, and most of these materials are either ferroelectric or antiferroelectric at low temperatures. In terms of the present energy-band results, one interesting group of compounds are those with lead atoms at the A sites ($PbTiO_3$, $PbZrO_3$, and $PbHfO_3$). Lead is believed to have a +2 charge in these compounds, which implies that the electronic configuration is $6s^2$. Unlike $SrTiO_3$ and $KTaO_3$, where the antibonding s-p bands are above the B-atom d bands and unoccupied, the lead-6s band must be below the titanium-3d bands in $PbTiO_3$ in order to explain the insulating properties of this compound.

It is interesting to estimate the position of the lead 6s band in $PbTiO_3$. To do this, we take the difference in the Herman and Skillman[18] one-electron energies for the strontium-5s and lead-6s orbitals, including relativistic effects. It is found that the lead-6s level is lower than the strontium-5s level by about 0.8 Ry or 11 eV. Since the bottom of the antibonding s-p band in $SrTiO_3$ is about 0.7 Ry above the oxygen-2p bands (Fig. 4), this estimate suggests that the lead-6s and oxygen-2p bands may overlap in $PbTiO_3$.

Another interesting group of compounds that are considered in Goodenough's survey are $LaRhO_3$, $LaCoO_3$, and $GdCoO_3$. These are semiconductors with band gaps of about 0.1 eV separating the filled t_{2g} and empty e_g conduction bands. We note in Figs. 3–6 that the present APW-LCAO band structures for these perovskite-type compounds consistently predict the existence of such a gap. The results of Table V indicate that this gap increases from 0.004 Ry in $KNiF_3$ to 0.020 Ry in $SrTiO_3$, 0.029 Ry in $KMoO_3$, and 0.056 Ry in $KTaO_3$. This is in contrast to the results of previous band-structure calculations for $SrTiO_3$[3,9] which predict overlapping e_g and t_{2g} bands.

We have previously considered the relationship between the energy levels of an isolated transition-metal complex and the corresponding energy-band states in the rocksalt and perovskite structures.[16] According to this analysis, the crystal field splitting Δ between the e_g and t_{2g} levels in an octahedral complex is given by

$$\Delta = E_{d\sigma} - E_{d\pi} + \tfrac{1}{2}(\Delta_s + \Delta_\sigma - \Delta_\pi) , \tag{4}$$

where, to lowest order,

$$\begin{aligned} \Delta_s &\approx 6[S_s E_{d\sigma} - (sd\sigma)]^2/(E_{d\sigma} - E_s) , \\ \Delta_\sigma &\approx 6[S_\sigma E_{d\sigma} - (pd\sigma)]^2/(E_{d\sigma} - E_{p\sigma}) , \\ \Delta_\pi &\approx 8[S_\pi E_{d\pi} - (pd\pi)]^2/(E_{d\pi} - E_{p\pi}) . \end{aligned} \tag{5}$$

These crystal field parameters affect the details of the antibonding d bands differently in the rocksalt and perovskite structures. In the rocksalt structure, there is no tendency for these crystal field parameters to split the e_g and t_{2g} bands, while in the perovskite structure, the e_g and t_{2g} bands are split if $(E_{d\sigma} - E_{d\pi} + \Delta_s) > \Delta_\pi$.

It is interesting to compare the APW-LCAO parameters for similar compounds with the rocksalt[15] and perovskite structures. The results of such a comparison are included in Table X. Here we compare the APW-LCAO parameters for two compounds in which the d electrons are itinerant (TiO and $SrTiO_3$) and two where the d electrons are believed to be localized (NiO and $KNiF_3$). We omit d-d interactions in this comparison because nearest-neighbor interactions in $KNiF_3$ correspond to second-neighbor interactions in NiO. The values for Δ_s, Δ_σ, and Δ_π for TiO and NiO have been determined from the results of Tables IV–VI in Ref. 15. The corresponding values for $SrTiO_3$ and $KNiF_3$ have been estimated from the energy-band results of Figs. 4 and 3, respectively.

Particularly in the perovskite structure where the nearest-neighbor metal-metal distance is large, the principal contribution to the antibonding d bandwidth arises from the nearest-neighbor

TABLE X. Comparison between the APW-LCAO parameters for TiO, $SrTiO_3$, NiO, and $KNiF_3$. Energy integrals are in rydbergs.

	TiO (a = 4.18 Å)		$SrTiO_3$ (a = 3.91 Å)		NiO (a = 4.20 Å)		$KNiF_3$ (a = 4.01 Å)	
	Energy	Overlap	Energy	Overlap	Energy	Overlap	Energy	Overlap
E_s	−1.103	1.000	−1.162	1.000	−1.167	1.000	−1.425	1.000
$(ss\sigma)$	−0.009	···	−0.010	···	−0.005	···	−0.003	···
$E_{p\sigma}$	−0.037	1.000	−0.058	1.000	−0.074	1.000	−0.057	1.000
$E_{p\pi}$	−0.037	1.000	−0.075	1.000	−0.074	1.000	−0.028	1.000
C_1	0.007	···	0.012	···	0.012	···	0.008	···
C_2	0.011	···	0.020	···	0.016	···	0.013	···
C_3	0.011	···	0.017	···	0.016	···	0.009	···
C_4	−0.004	···	−0.004	···	−0.005	···	−0.002	···
$E_{d\sigma}$	0.779	1.000	0.466	1.000	0.374	1.000	0.570	1.000
$E_{d\pi}$	0.817	1.000	0.466	1.000	0.385	1.000	0.570	1.000
$(sd\sigma), S_s$	−0.169	0.051	−0.183	0.043	−0.089	0.043	−0.085	0.028
$(pd\sigma), S_\sigma$	−0.124	0.086	−0.156	0.078	−0.076	0.053	−0.077	0.047
$(pd\pi), S_\pi$	0.057	−0.026	0.076	−0.058	0.035	−0.031	0.038	−0.018
Δ_s	0.135		0.159		0.044		0.033	
Δ_σ	0.262		0.371		0.122		0.109	
Δ_π	0.051		0.139		0.031		0.029	

overlap-covalency interactions [S_s, $(sd\sigma)$, etc.]. These are much stronger in the itinerant (TiO, $SrTiO_3$) than the localized (NiO, $KNiF_3$) systems. It is interesting to note that for either pair of compounds, one could generate a reasonable model for the perovskite band structure using the rocksalt LCAO parameters or vice versa. The fact that $(E_{d\sigma} - E_{d\pi} + \Delta_s) > \Delta_\pi$ for both TiO and NiO shows that these LCAO parameters that are derived from APW calculations for the rocksalt structure where the e_g and t_{2g} bands overlap predict nonoverlapping e_g and t_{2g} bands in the perovskite structure.

In TiO and NiO, the oxygen sites have full cubic symmetry so that the orbital energies $E_{p\sigma}$ and $E_{p\pi}$ are identical. In the perovskite structure, the tetragonal symmetry at the C-atom sites causes a splitting between $E_{p\sigma}$ and $E_{p\pi}$. It is expected that $E_{p\sigma} < E_{p\pi}$, and this is found to be the case in $KNiF_3$ but not in $SrTiO_3$ (or the other oxides, according to the results in Table VI). It is believed that this discrepancy is due to the fact that the present simplified LCAO model neglects the metal s-p antibonding conduction bands in the LCAO fit to the APW results.

A similar splitting in the orbital energies for the $e_g(E_{d\sigma})$ and t_{2g} $(E_{d\pi})$ states is expected in both structures. In an octahedral environment, it is expected that $E_{d\sigma} < E_{d\pi}$,[15] and the energy difference $\gamma \equiv E_{d\sigma} - E_{d\pi}$ is often referred to as the Kleiner correction[74] in the ligand-field literature. According to the results in Table X, γ is about − 0.038 Ry in TiO and − 0.011 Ry in NiO. As mentioned in Sec. IIC, we were unable to determine $E_{d\sigma}$ in the present application of the APW-LCAO method to the perovskite-type compounds. We have arbitrarily set $\gamma = 0$ so that $E_{d\sigma} = E_{d\pi} = E_d$. As a result of this simplification, it is expected that the present values for $(sd\sigma)$, S_s, and Δ_s underestimate the actual values of these parameters.

We can best compare the various band-structure models for these perovskite-type compounds in terms of the LCAO parameters that are involved in each model. The results of such a comparison for $SrTiO_3$ are contained in Table XI and for $KNiF_3$ in Table XII. In Table XI, we compare the APW-LCAO parameters for $SrTiO_3$ with those of KL[3] and Soules *et al.*[9] (SKVR). In Table XII, the APW-LCAO parameters for $KNiF_3$ are compared with the MO integrals of Sugano and Shulman[34] (SS). In the case of the KL and SS integrals, the zero of energy has been adjusted so that it coincides with the top of the 2p valence band at the zone center.

There are several differences in sign between the APW-LCAO and KL parameters for $SrTiO_3$. There is a systematic sign difference in the case

TABLE XI. Comparison between the APW-LCAO parameters for $SrTiO_3$ and the tight-binding integrals of Kahn and Leyendecker (KL) and Soules *et al.* (SKVR). Energy integrals are in rydbergs.

LCAO	APW-LCAO		KL		SKVR	
Parameter	Energy	Overlap	Energy	Overlap	Energy	Overlap
E_s	−1.162	1.000	···	···	−1.950	1.000
$(ss\sigma)$	−0.010	···	···	···	−0.061	0.009
$E_{p\sigma}$	−0.060	1.000	−0.060	1.000	−0.604	1.000
$E_{p\pi}$	−0.075	1.000	−0.025	1.000	−0.544	1.000
C_1	0.012	···	−0.004	···	0.038	−0.023
C_2	0.020	···	−0.008	···	0.080	−0.033
C_3	0.017	···	−0.008	···	0.061	−0.033
C_4	−0.003	···	0.004	···	−0.047	0.010
$E_{d\pi}$	0.466	1.000	0.217	1.000	0.574	1.000
$E_{d\sigma}$	0.466	1.000	0.263	1.000	0.114	1.000
$(sd\sigma), S_s$	−0.183	0.043	···	···	−0.353	0.129
$(pd\sigma), S_\sigma$	−0.156	0.078	0.154	···	−0.308	0.139
$(pd\pi), S_\pi$	0.076	−0.058	0.062	···	0.163	−0.088

TABLE XII. Comparison between the APW-LCAO parameters for $KNiF_3$ and MO integrals of Sugano and Shulman (SS). Energy integrals are in rydbergs.

	APW-LCAO		SS	
Parameter	Energy	Overlap	Energy	Overlap
E_s	−1.425	1.000	−1.825	1.000
$E_{p\sigma}$	−0.058	1.000	−0.159	1.000
$E_{p\pi}$	−0.028	1.000	0.000	1.000
$E_{d\sigma}$	0.570	1.000	0.440	1.000
$E_{d\pi}$	0.570	1.000	0.407	1.000
$(sd\sigma), S_s$	−0.085	0.028	−0.126	0.047
$(pd\sigma), S_\sigma$	−0.077	0.047	−0.103	0.064
$(pd\pi), S_\pi$	0.038	−0.018	−0.038	0.038

of the nearest-neighbor oxygen-$2p$ interaction parameters, $C_1 - C_4$. KL treat these interactions in the two-center approximation and state that their values for $(pp\sigma)$ and $(pp\pi)$ are taken from Switendick's NiO calculation.[75] In fact, KL have reversed the signs of both $(pp\sigma)$ and $(pp\pi)$ and reduced the magnitude of $(pp\sigma)$, apparently by using Switendick's value of $E_{x,x}(\frac{1}{2}, \frac{1}{2}, 0) = \frac{1}{2}(pp\sigma) + \frac{1}{2}(pp\pi)$ for $(pp\sigma)$. If the actual values for Switendick's integrals are applied to calculate C_1-C_4, one obtains $C_1 = 0.012$ Ry, $C_2 = 0.016$ Ry, $C_3 = 0.016$ Ry, and $C_4 = -0.005$ Ry, which are in good agreement with the APW-LCAO values for $SrTiO_3$ in Table XI. These discrepancies are the source of the main differences between the KL oxygen-$2p$ bands and the present APW-LCAO results.

Because there is an arbitrary phase factor associated with both the metal and ligand orbitals, the relative signs of the various covalency parameters $(sd\sigma)$, $(pd\sigma)$, and $(pd\pi)$ are arbitrary in the cubic perovskite structure. The LCAO energy-band results are independent of these signs, though they do require that a given pair of overlap-covalency parameters [S_s, $(sd\sigma)$, etc.] have opposite signs.[14] If the radial functions for the e_g and t_{2g} orbitals are equal (or have identical phase factors), then $(pd\sigma)$ and $(pd\pi)$ will have opposite signs. It is found that when spin-orbit effects are included in the LCAO secular equation, the energy-band results depend to a small degree on the relative signs of these covalency parameters. This is due to the fact that the spin-orbit effects couple the d states in the otherwise independent e_g and t_{2g} manifolds. The relative signs of the $(pd\sigma)$ and $(pd\pi)$ covalency parameters play an important role in the LCAO treatment of tetragonal $SrTiO_3$, as discussed in the following paper.

The magnitudes of the nearest-neighbor interactions in the SKVR and SS molecular-orbital calculations are significantly larger than the corresponding APW-LCAO results. This implies that the radial functions for their ligand $2s$ and $2p$ (and possibly the metal $3d$) orbitals are more extended than the "effective" orbitals in the APW-LCAO model. A similar effect has been observed previously[15] in a comparison between the APW-LCAO parameters for VO and the first-principles LCAO integrals of Norwood and Fry.[76] This seems to suggest that atomic or ionic orbitals do not represent an ideal set of basis functions for LCAO or MO calculations of the valence and conduction bands in solids. It is also possible that the present APW-LCAO method yields "effective" nearest-neighbor interactions that are reduced by cancellation effects involving more distant shells of neighboring atoms.

Because of these large nearest-neighbor interactions, the SKVR calculation predicts large bandwidths for $SrTiO_3$. The SKVR oxygen-$2s$ bandwidth is five times larger than the APW-LCAO results, as expected from the relative values for $(ss\sigma)$ in Table XI. Their oxygen-$2p$ and titanium-t_{2g} and -e_g bandwidths are twice the APW values.

In the SKVR calculation for $SrTiO_3$, the energy difference $E_{d\sigma} - E_{d\pi}$ is quite large (−0.46 Ry) compared to the SS value (−0.03 Ry) for $KNiF_3$. The opposite is true for the $E_{p\sigma} - E_{p\pi}$ splittings, where SKVR obtain a smaller splitting (−0.06 Ry) than SS (−0.16 Ry). In $KNiF_3$, this $E_{p\sigma} - E_{p\pi}$ splitting is sufficient to separate the fluorine $2p\sigma$ and $2p\pi$ valence bands into nonoverlapping subbands (see Fig. 5 of Ref. 14). This is contrary to the present APW results for $KNiF_3$.

Both KL and SKVR have attempted to estimate the positions of the strontium and titanium s-p conduction-band states in $SrTiO_3$. They suggest that these bands are 10-15 eV above the titanium-$3d$ bands. The present results suggest that these s-p bands and the strontium-$4d$ bands are low enough in energy so that they overlap the titanium-e_g bands. The optical data for $SrTiO_3$, $KTaO_3$, and ReO_3 suggest that these bands fall about 8–10 eV above the oxygen-$2p$ valence bands or 5–8 eV lower than the KL and SKVR estimates.

Šroubek[61] has criticized several aspects of the KL model and has suggested a revised model for the $SrTiO_3$ conduction bands. Šroubek estimates that $E_{d\sigma} - E_{d\pi} \approx -0.8$ eV and $\Delta_s \approx 0.5$ eV in $SrTiO_3$, so that the conduction-band minima along $\langle 100 \rangle$ involve the $\Delta_2(e_g)$ rather than the $\Delta_{2'}(t_{2g})$ orbitals (see Fig. 10). He argues that since the $\Delta_2(e_g)$ band interacts with the oxygen-$2s$ orbitals, it will have a greater width than the $\Delta_{2'}$ band (which does not), thereby explaining the small values for the DS effective mass that he infers from his tunneling data.

The present APW-LCAO results for $SrTiO_3$ as well as the other perovskite-type compounds indicate that Šroubek has grossly underestimated the magnitude of Δ_s. The present APW-LCAO calculations indicate that $\Delta_s \approx 2$ eV. The self-consistent MO calculation by SKVR suggests that Δ_s

= 6.6 eV. Both calculations predict that the lowest conduction-band states involve the titanium-t_{2g} rather than the-e_g orbitals. Furthermore, it is clear from the results shown in Figs. 2–6 and Fig. 10 that the $\Delta_2(e_g)$ and $\Delta_{2'}(t_{2g})$ bandwidths are comparable in all these compounds. This is due to the fact that the s-d overlap-covalency interaction is constant along the entire $\Delta_2(e_g)$ band from Γ and X when nearest-neighbor oxygen-titanium interactions are considered. As a result, the widths of both the $\Delta_2(e_g)$ and $\Delta_{2'}(t_{2g})$ bands are due primarily to nearest-neighbor d-d interactions. If the $(dd\delta)$ integrals for the e_g and t_{2g} orbitals (D_6 and D_3 of Table VI, respectively) are assumed to be equal, then the total $\Delta_2(e_g)$ and $\Delta_{2'}(t_{2g})$ bandwidths are both equal to $4(dd\delta)$.

This brings us to the important question concerning the location of the conduction-band minima in $SrTiO_3$ and $KTaO_3$. In every case, the APW results predict that the minimum occurs at Γ rather than at X. Within the LCAO model, the location of the conduction-band minimum depends on the sign of D_3 in Table VI, or $(dd\delta)$ in the two-center approximation. To the author's knowledge, all direct calculations of $(dd\delta)$[76,77] and most LCAO[13,15] and combined interpolation schemes[78] (for transition metals as well as compounds) predict that $(dd\delta)$ is small and negative. Thus, it was anticipated that the present APW calculations would predict $E(\Gamma_{25'}) < E(X_3)$. Although the calculated energy difference, $E(X_3) - E(\Gamma_{25'})$, is quite small (0.19 eV) in $SrTiO_3$, it is believed to be quite reliable. Its magnitude could possibly vary if a self-consistent calculation were performed, but it is unlikely that its sign would change.

Detailed calculations were performed to determine the extent to which the incomplete convergence of the APW wave functions could affect the $\Delta_{2'}$ bandwidth in these compounds. These studies revealed that the APW eigenvalues converge much more slowly when the corrections to the muffin-tin potential $V_\Delta(\vec{r})$ are included in the calculation. Both $E(\Gamma_{25'})$ and $E(X_3)$ decrease by a few thousandths of a rydberg when the total number of APW basis functions is increased from about 250 to 400. However, the energy difference $E(X_3) - E(\Gamma_{25'})$ is reduced only slightly, from 0.0139 Ry for 250 basis functions to 0.0120 Ry for 400 APW's. It is believed that convergence errors will not alter the prediction that the conduction-band minima in $SrTiO_3$ and $KTaO_3$ are at Γ.

The APW calculations for $SrTiO_3$ and $KTaO_3$ predict direct band gaps of about 6.2 eV for both compounds. These are about twice the observed gaps. It is found that APW calculations for transition-metal compounds that are based on superimposed atomic potentials usually tend to overestimate these p-d band gaps.[13,15,16] Schwartz[79] has suggested that this may be due to a combination of self-consistency and exchange effects. In a self-consistent APW calculation for NbN[80] involving Slater's $X\alpha$ method,[81] Schwartz finds that the niobium $4d$ bands are located 0.3 Ry lower in energy relative to the nitrogen $2p$ bands than they are in a similar calculation based on superimposed atomic potentials.[82] Schwartz finds that one-third of this shift is the result of using $\alpha \approx 0.7$ (rather than 1, as we have assumed in the present study). The remaining shift of 0.2 Ry in Schwartz's calculation occurs when the calculations are iterated to produce a self-consistent potential. Thus, the present overestimate of the $SrTiO_3$ and $KTaO_3$ band gaps is easily accounted for in this manner. SKVR,[9] Šimánek and Šroubek,[83] and Fowler[84] suggest that the $SrTiO_3$ one-electron band gap should be much larger than that suggested by the optical data. They attribute the difference to polarization effects or excitons. Slater and Wood[85] also suggest that optical absorption in insulating crystals should be treated as localized excitations in the $X\alpha$ method. Although these effects are undoubtedly important in understanding the optical properties of $KNiF_3$, it is not yet clear whether they play a similar role in $SrTiO_3$, $KTaO_3$, and ReO_3.

ACKNOWLEDGMENTS

I have had the benefit of numerous discussions and conversations with many of my colleagues on various aspects of this investigation, particularly A. S. Barker, C. N. Berglund, J. R. Brews, R. E. Dietz, L. R. Testardi, W. M. Walsh, Jr., and S. H. Wemple. My original interest in $SrTiO_3$ dates back to discussions with M. L. Cohen concerning superconductivity and the band structure of $SrTiO_3$. I have enjoyed useful conversations with S. K. Kurtz concerning the interpretation of his reflectivity data. I am grateful to J. K. Hulm and J. L. Richardson for providing preprints of their unpublished work on $SrTiO_3$.

[1] J. B. Goodenough and J. M. Longo, in *Landolt-Bornstein Tabellen*, edited by K. H. Hellwege and A. M. Hellwege (Springer-Verlag, Berlin, 1970).

[2] R. Abe *et al.*, in Ref. 1.

[3] A. H. Kahn and A. J. Leyendecker, Phys. Rev. 135, A1321 (1964).

[4] J. F. Schooley, W. R. Hosler, and M. L. Cohen, Phys. Rev. Letters 12, 474 (1964).

[5] J. C. Slater and G. F. Koster, Phys. Rev. 94, 1498 (1954).

[6] M. L. Cohen, Phys. Rev. 134, A511 (1964).

[7] Two of the most recent papers are B. Kleinman and M. Karplus, Phys. Rev. B 3, 24 (1971); T. F. Soules, J. W. Richardson, and D. M. Vaught, Phys. Rev. B 3,

2186 (1971). These papers contain references to the earlier molecular-orbital calculations on the $(NiF_6)^{4-}$ complex.

[8]F. W. Lytle, J. Appl. Phys. 35, 2212 (1964).

[9]T. F. Soules, E. J. Kelly, D. M. Vaught, and J. W. Richardson, Phys. Rev. B 6, 1519 (1972); J. W. Richardson, E. J. Kelly, T. F. Soules, and D. M. Vaught, Bull. Am. Phys. Soc. 16, 371 (1971).

[10]S. M. Marcus and T. A. Bither, Phys. Rev. Letters 23, 1381 (1969).

[11]S. M. Marcus, Phys. Letters 27A, 584 (1968).

[12]J. E. Graebner and E. S. Greiner, Phys. Rev. 185, 992 (1969).

[13]L. F. Mattheiss, Phys. Rev. 181, 987 (1969).

[14]L. F. Mattheiss, Phys. Rev. B 2, 3918 (1970).

[15]L. F. Mattheiss, Phys. Rev. B 5, 290 (1972).

[16]L. F. Mattheiss, Phys. Rev. B 5, 306 (1972).

[17]L. F. Mattheiss, following paper, Phys. Rev. B 6, 4740 (1972).

[18]F. Herman and S. Skillman, *Atomic Structure Calculations* (Prentice-Hall, Englewood Cliffs, N. J., 1963).

[19]J. C. Slater, Phys. Rev. 81, 385 (1951).

[20]L. F. Mattheiss, J. H. Wood, and A. C. Switendick, in *Methods in Computational Physics*, edited by B. Alder, S. Fernbach, and M. Rotenberg (Academic, New York, 1968).

[21]G. Dresselhaus, A. F. Kip, and C. Kittel, Phys. Rev. 98, 368 (1955).

[22]L. F. Mattheiss, Phys. Rev. B 1, 373 (1970).

[23]A. Okazaki, Y. Suemune, and T. Fuchikami, J. Phys. Soc. Japan 14, 1823 (1959).

[24]S. Sugano, Y. Tanabe, and H. Kamimura, *Multiplets of Transition-Metal Ions in Crystals* (Academic, New York, 1970).

[25]V. Heine and L. F. Mattheiss, J. Phys. C 4, L191 (1971).

[26]V. W. Rüdorff, J. Känder, and D. Babel, Z. Anorg. Allgem. Chem. 317, 261 (1962).

[27]W. Low, Phys. Rev. 109, 247 (1958).

[28]R. Newman and R. M. Chrenko, Phys. Rev. 114, 1507 (1959).

[29]K. Knox, R. G. Shulman, and S. Sugano, Phys. Rev. 130, 506 (1963).

[30]M. Balkanski, P. Moch, and R. G. Shulman, J. Chem. Phys. 40, 1897 (1964).

[31]J. Ferguson, H. J. Guggenheim, and D. L. Wood, J. Chem. Phys. 40, 822 (1964).

[32]J. Ferguson and H. J. Guggenheim, J. Chem. Phys. 44, 1095 (1966).

[33]J. Ferguson, H. J. Guggenheim, H. Kamimura, and Y. Tanabe, J. Chem. Phys. 42, 775 (1965).

[34]S. Sugano and R. G. Shulman, Phys. Rev. 130, 517 (1963).

[35]J. Ferguson, Australian J. Phys. 21, 323 (1968).

[36]R. J. Powell and W. E. Spicer, Phys. Rev. B 2, 2182 (1970).

[37]P. Hagenmuller, in *Progress in Solid State Chemistry*, edited by H. Reiss (Pergamon, Oxford, England, 1971), Vol. 5.

[38]T. A. Bither, J. L. Gillson, and H. S. Young, Inorg. Chem. 5, 1559 (1966).

[39]H. P. R. Frederikse, W. R. Hosler, and W. R. Thurber, J. Phys. Soc. Japan Suppl. 21, 32 (1966).

[40]H. P. R. Frederikse, in *Electronic Structures in Solids*, edited by E. D. Haidemenakis (Plenum, New York, 1969).

[41]H. P. R. Frederikse, W. R. Thurber, and W. R. Hosler, Phys. Rev. 134, A442 (1964).

[42]S. H. Wemple, Phys. Rev. 137, A1575 (1965).

[43]M. Cardona, Phys. Rev. 140, A651 (1965).

[44]S. K. Kurtz, in *Proceedings of the International Meeting on Ferroelectricity*, edited by V. Dvořak, A. Fouskova, and P. Glogar (Institute of Physics, Czechoslovak Academy of Sciences, Prague, 1966).

[45]S. K. Kurtz, T. C. Rich, and W. J. Cole (unpublished).

[46]D. Brust, Phys. Rev. 134, A1337 (1964).

[47]J. Feinleib, W. J. Scouler, and A. Ferretti, Phys. Rev. 165, 765 (1968).

[48](a) J. A. Noland, Phys. Rev. 94, 724 (1954); (b) W. S. Baer, *ibid.* 144, 734 (1966); (c) Y. T. Sihvonen, J. Appl. Phys. 38, 4431 (1967); (d) M. I. Cohen and R. F. Blunt, Phys. Rev. 168, 929 (1968); (e) M. Capizzi and A. Frova, Phys. Rev. Letters 25, 1298 (1970); Nuovo Cimento 5, 181 (1971); (f) K. W. Blazey, Phys. Rev. Letters 27, 146 (1971); (g) D. Redfield and W. Burke, *ibid.* 28, 435 (1972).

[49]W. S. Baer, J. Phys. Chem. Solids 28, 667 (1967).

[50](a) A. Frova and P. J. Boddy, Phys. Rev. 153, 606 (1967); (b) M. DiDomenico, Jr. and S. H. Wemple, *ibid.* 166, 565 (1968).

[51]R. H. Tredgold and R. H. Williams, J. Phys. Soc. Japan 21S, 56 (1966).

[52]G. F. Derbenwick, Stanford University Solid State Electronics Lab. Technical Report No. 5220-2, 1970 (unpublished).

[53]M. A. Blokhin and A. T. Shuvaev, Bull. Acad. Sci. USSR, Physical Series 26, 429 (1962) (Columbia Technical Translations).

[54]L. S. Senhouse, G. E. Smith, and M. V. DePaolis, Phys. Rev. Letters 15, 776 (1965).

[55]H. P. R. Frederikse and G. A. Candela, Phys. Rev. 147, 583 (1966).

[56]E. Ambler, J. H. Colwell, W. R. Hosler, and J. F. Schooley, Phys. Rev. 148, 280 (1966).

[57]A. S. Barker, Jr., in *Optical Properties and Electronic Structure of Metals and Alloys*, edited by F. Abelès (North-Holland, Amsterdam, 1966).

[58]W. S. Baer, Phys. Rev. Letters 16, 729 (1966).

[59]H. P. R. Frederikse, W. R. Hosler, W. R. Thurber, J. Babiskin, and P. G. Siebermann, Phys. Rev. 158, 775 (1967).

[60]N. E. Phillips, B. B. Triplett, R. D. Clear, H. E. Simon, J. K. Hulm, C. K. Jones, and R. Mazelsky, in *Proceedings of the International Conference on the Science of Superconductivity*, edited by F. Chilton (North-Holland, Amsterdam, 1971).

[61]Z. Šroubek, Phys. Rev. B 2, 3170 (1970).

[62]K. W. Johnson and D. H. Olsen, Phys. Rev. B 3, 1244 (1970).

[63]W. M. Walsh, Jr., L. W. Rupp, Jr., P. S. Peercy, and L. F. Mattheiss, Bull. Am. Phys. Soc. 17, 302 (1972).

[64]B. Lax and J. G. Mavroides, in *Solid State Physics*, edited by F. Seitz and D. Turnbull (Academic, New York, 1960).

[65]D. M. Eagles, Phys. Status Solidi 48, 407 (1971).

[66]H. P. R. Frederikse, W. R. Hosler, and W. R. Thurber, Phys. Rev. 143, 648 (1966).

[67]O. N. Tufte and E. L. Stelzer, Phys. Rev. 173, 775 (1968).

[68]I. Camlibel (unpublished).

[69]W. R. Hosler and H. P. R. Frederikse, Solid State

Commun. 7, 1443 (1969).
[70]J. G. Mavroides and B. Lax, Phys. Rev. 107, 1530 (1957).
[71]O. N. Tufte and E. L. Stelzer, Phys. Rev. 141, 675 (1966).
[72]H. P. R. Frederikse, W. R. Hosler, and R. C. Casella, in *Proceedings of the Ninth International Conference on the Physics of Semiconductors*, edited by S. M. Ryukin (Nauka, Leningrad, 1968).
[73]J. B. Goodenough, in Ref. 37.
[74]W. H. Kleiner, J. Chem. Phys. 20, 1784 (1952).
[75]A. C. Switendick, MIT Solid-State and Molecular Theory Group Quarterly Progress Report No. 49, 1963 (unpublished).
[76]T. E. Norwood and J. L. Fry, Phys. Rev. B 2, 472 (1970).
[77]See for example, J. M. Tyler, T. E. Norwood, and J. L. Fry, Phys. Rev. B 1, 297 (1970).
[78]L. Hodges, H. Ehrenreich, and D. N. Lang, Phys. Rev. 152, 505 (1966); F. M. Mueller, *ibid.* 153, 659 (1967).
[79]K. Schwartz (private communication).
[80]K. Schwartz, Monatsh. Chem. 102, 1400 (1971).
[81]J. C. Slater, in *Computational Methods in Band Theory*, edited by P. M. Marcus, J. F. Janak, and A. R. Williams (Plenum, New York, 1971).
[82]L. F. Mattheiss, Phys. Rev. B 5, 315 (1972).
[83]E. Šimánek and Z. Šroubek, Phys. Status Solidi 8, K47 (1965).
[84]W. B. Fowler, Phys. Rev. 151, 657 (1966).
[85]J. C. Slater and J. H. Wood, Intern. J. Quantum Chem. 4, 3 (1971).

PHYSICAL REVIEW B VOLUME 6, NUMBER 12 15 DECEMBER 1972

Effect of the 110 °K Phase Transition on the $SrTiO_3$ Conduction Bands

L. F. Mattheiss
Bell Laboratories, Murray Hill, New Jersey 07974
(Received 26 May 1972)

The linear-combination-of-atomic-orbitals (LCAO) model of the preceding paper for the cubic-$SrTiO_3$ band structure is applied to predict the effect of the 110 °K phase transition on the $SrTiO_3$ conduction bands. In this cubic-to-tetragonal structural transformation, neighboring octahedral TiO_6 complexes are rotated rigidly in opposite directions about the c axis through small angles $\pm\varphi$. This LCAO approach is expected to be accurate since nearest-neighbor distances and bond angles are unchanged in this transition. This enables one to apply the LCAO parameters for cubic $SrTiO_3$ to predict the band structure in the tetragonal state. The effects of the tetragonal distortion are introduced into the LCAO secular equation as small changes in the cubic structure factors, $e^{i\vec{k}\cdot\vec{R}_j}$. Neglecting spin-orbit coupling, this model predicts a splitting of the $\Gamma_{25'}$ conduction-band minimum by an energy proportional to φ^2. At 4.2 °K, where $c/a = 1.0006$ and $\varphi = 2.1°$, $\Gamma_{25'}$ is split by about 90 meV into a lower doubly degenerate Γ_5^+ state and an upper nondegenerate Γ_4^+ state. Spin-orbit coupling further splits the Γ_5^+ state by an energy comparable with the titanium $3d$ spin-orbit parameter, $\xi_{3d} \approx 25$ meV. This produces a warped single-valley model for the $SrTiO_3$ conduction bands at low carrier densities n and a two-band model containing "heavy" and "light" electrons for $n > 10^{19}$ cm^{-3}. It is shown that the splitting of the conduction-band minimum in $SrTiO_3$ is similar in magnitude but opposite in sign to that caused by the ferroelectric transition in $BaTiO_3$.

I. INTRODUCTION

In the preceding paper[1] (hereafter referred to as I), the nonrelativistic augmented-plane-wave (APW) method has been combined with the linear-combination-of-atomic-orbitals (LCAO) interpolation scheme to determine the band structures for several "ideal" cubic perovskite-type compounds, including $KNiF_3$, $SrTiO_3$, $KMoO_3$, and $KTaO_3$. These calculations predict that the conduction-band minima for $SrTiO_3$ and $KTaO_3$ consist of warped bands at the zone center Γ rather than many valleys at or near the Brillouin-zone boundaries along the ⟨100⟩ directions, as Kahn and Leyendecker[2] have proposed. At the moment, there is no decisive experimental data for either compound that can distinguish between these warped-band and many-valley models.

In the case of $SrTiO_3$, the interpretation of the low-temperature data is complicated by the occurrence of a cubic-to-tetragonal phase transition at about 110 °K, plus the possibility of additional structural transformations at lower temperatures.[3] Unoki and Sakudo[4] have identified the space group of the tetragonal phase below 110 °K as D_{4h}^{18} using electron-spin-resonance techniques. They find no evidence for a further reduction in symmetry down to 4.2 °K. However, in a recent study involving monodomain samples, Sakudo and Unoki[5] observe a dielectric anisotropy within the plane perpendicular to the c axis below 65 °K, and this suggests that $SrTiO_3$ possesses orthorhombic or lower symmetry in this temperature range.

According to Lytle's x-ray data,[3] the c/a ratio